CHAPTER ELEVEN

Deciphering lipid transfer between and within membranes with time-resolved small-angle neutron scattering

Ursula Perez-Salas^{a,*}, Sumit Garg^a, Yuri Gerelli^b, and Lionel Porcar^c

Contents

1.	Introduction					
2.	Small angle neutron scattering (SANS) in the study of membranes					
	2.1 SANS nuts and bolts	362				
	2.2 Contrast and contrast matching	366				
	2.3 Time-resolved small angle neutron scattering (TR-SANS)	368				
	2.4 Measurement of the transfer of lipids and sterols between membranes					
	using TR-SANS	369				
3.	Kinetic and thermodynamic characteristics of the transport of lipids and sterols					
	between and within membranes obtained from TR-SANS measurements					
	3.1 Obtaining transfer coefficients: Exchange and flip-flop of lipids and sterols					
	in membranes	375				
	3.2 Obtaining the energetics of lipid and sterol transport	379				
4.	Transport behavior of lipids and sterols in membranes					
	4.1 Exchange and flip-flop behavior of lipids in model membranes	381				
	4.2 Exchange and flip-flop behavior of sterols in model membranes	385				
	4.3 Decoupling exchange from flip-flop	391				
	4.4 Lipid exchange and flip-flop behavior in the presence of biological agent	s 396				
5.	Current and future perspectives	400				
Ac	Acknowledgments					
Re	References					

Abstract

This review focuses on time-resolved neutron scattering, particularly time-resolved small angle neutron scattering (TR-SANS), as a powerful in situ noninvasive technique to investigate intra- and intermembrane transport and distribution of lipids and sterols in lipid membranes. In contrast to using molecular analogues with potentially large

^aPhysics Department, University of Illinois at Chicago, Chicago, IL, United States

^bDepartment of Life and Environmental Sciences, Universita' Politecnica delle Marche, Ancona, Italy

^cInstitut Laue Langevin, Grenoble Cedex 9, France

^{*}Corresponding author: e-mail address: ursulaps@uic.edu

chemical tags that can significantly alter transport properties, small angle neutron scattering relies on the relative amounts of the two most abundant isotope forms of hydrogen: protium and deuterium to detect complex membrane architectures and transport processes unambiguously. This review discusses advances in our understanding of the mechanisms that sustain lipid asymmetry in membranes—a key feature of the plasma membrane of cells—as well as the transport of lipids between membranes, which is an essential metabolic process.

Abbreviation

AMP antimicrobial peptide CM contrast matched

DMPC 1,2-dimyristoyl-*sn*-glycero-3-phosphocholine **DPPC** 1,2-dipalmitoyl-*sn*-glycero-3-phosphocholine

HDL high density lipoproteins
LDL low density lipoproteins
MD molecular dynamics
NMR nuclear magnetic resonance
NR neutron reflectivity

POPA 1-palmitoyl-2-oleoyl-glycero-3-phosphatidic acid POPC 1-palmitoyl-2-oleoyl-glycero-3-phosphocholine POPG 1-palmitoyl-2-oleoyl-sn-glycero-3-phosphoglycerol

SANS small-angle neutron scattering
SAXS small-angle X-ray scattering
SLD scattering length density

TR-NR time-resolved neutron reflectivity

TR-SANS time-resolved small-angle neutron scattering

1. Introduction

Lipids are essential components of cellular membranes (Yeagle, 1993). The structure of membranes consists of a continuous double layer (bilayer) of lipid molecules in which membrane proteins are embedded. Cells use this structure as the boundary that separates their interior from the environment that surrounds them (the extracellular space). Eukaryotic cells also bound organelles, having specialized functions, with membranes that require unique protein and lipid compositions (van Meer, Voelker, & Feigenson, 2008). Further, some of these membranes, like the cell's boundary, the plasma membrane (PM), are known to have a strict asymmetric distribution of lipids between the cytosolic facing leaflet and the extracellular facing leaflet and this distribution is responsible for the physiological

fate of cells (Bretscher, 1972; Kobayashi & Menon, 2018; Opdenkamp, 1979; van Meer et al., 2008). For example, serine lipids, normally in the inner cytosolic facing leaflet, when present in the outer exocellular leaflet, signal for phagocytosis and blood coagulation (Fadok et al., 1992).

Indeed, transbilayer flip-flop rates and energetics can influence interorganelle lipid transport by rearranging lipids from inner to outer leaflets or vice versa; this directly affects membrane curvature, for example, and consequently vesicle budding and fission and vesicle fusion (Lev, 2006; Sprong, van der Sluijs, & van Meer, 2001). In addition to an asymmetric distribution of lipids across membranes, the distribution of molecular components in membranes can be laterally heterogeneous (Devaux & Morris, 2004; Gupta, Korte, Herrmann, & Wohland, 2020; Simons & Ikonen, 1997) and implicated in signaling processes through the PM (Carbone et al., 2017; Stone, Shelby, Nunez, Wisser, & Veatch, 2017; Xiao, McAtee, & Su, 2021).

As a result, the quest to understand lipid trafficking as it relates to lipid homeostasis and metabolism, and how this lipid organization leads to proper membrane function, has been the focus of numerous studies for half a century (Holthuis & Levine, 2005; Nicolson, 2014). These studies have lead to significant breakthroughs, including those that lead to the 2013 Nobel Award in Medicine and Physiology for the finding that vesicular transport plays a major part in protein and lipid translocation along several energy-dependent pathways (Mellman & Emr, 2013). Further, it was discovered that nonvesicular transport mechanisms, including the spontaneous movement of lipids, also play critical roles in lipid homeostasis (Lev, 2010) as demonstrated by the existence of such transport, even under conditions in which vesicular transport is blocked (Kaplan & Simoni, 1985; Vance, Aasman, & Szarka, 1991).

One way to gauge the energetic toll of lipid transport is to quantify the passive movement of lipids between and within membranes. Unfortunately, the field has moved slowly due to the wide variation in the rates of lipid transfer between and particularly within membranes. Even in studies of model membrane systems, where lipid composition is controlled, the reported transfer rates have been inconsistent. For example, the reported half-life for cholesterol's transmembrane flipping varies by five to six orders of magnitude, ranging from several hours (Brasaemle, Robertson, & Attie, 1988; Poznansky & Lange, 1978; Rodrigueza, Wheeler, Klimuk, Kitson, & Hope, 1995) to a few minutes or seconds (Backer & Dawidowicz, 1981; John, Kubelt, Muller, Wustner, & Herrmann, 2002;

Leventis & Silvius, 2001; Schroeder et al., 1996; Steck, Ye, & Lange, 2002), and to even a few milliseconds (Baral, Levental, & Lyman, 2020; Bruckner, Mansy, Ricardo, Mahadevan, & Szostak, 2009) to tens of nanoseconds (Bennett, MacCallum, Hinner, Marrink, & Tieleman, 2009; Gu, Baoukina, & Tieleman, 2019). Noninvasive approaches like time-resolved small angle neutron scattering (TR-SANS) or sum-frequency generation vibrational spectroscopy (SFGVP) have shown that the movement of lipids is extremely sensitive to slight chemical structure differences, finding that the transfer rates of unaltered lipid molecules are dramatically different from their chemically tagged counterparts (for example, due to a fluorescent label) (Garg, Porcar, Woodka, Butler, & Perez-Salas, 2011; Liu & Conboy, 2005). Even studies using the same lipids and similar time resolved noninvasive approaches to investigate the movement of lipids across the bilayer (flip-flop) found drastically different results: in single flat supported membranes flipflop of lipids are found to be several orders of magnitude faster (Anglin & Conboy, 2009; Gerelli, Porcar, Lombardi, & Fragneto, 2013) than in vesicles, which are reported to take hours (Liu, Kelley, Batchu, Porcar, & Perez-Salas, 2020; Marquardt et al., 2017; Nakano, Fukuda, Kudo, Endo, & Handa, 2007). As it turned out, the surface supporting the membranes produce membrane defects (Marquardt et al., 2017), as well as a broadening of the melting phase transition of lipids (Gerelli, 2019) and surface driven lipid packing constraints (Wah et al., 2017) that promote fast flip-flop.

The past decade and in particular the past 5 years have seen progress in the revision of protocols to remove possible artifacts and biases that may be responsible for these hugely varying reports. Indeed, it became clear that the use of chemical tags, extraneous compounds, and even a supporting surface affect or influence lipid transport. Hence the use of nonperturbing approaches has become a strict requirement for a detailed study of the behavior of lipids in membranes. As a result, neutron scattering and in particular TR-SANS coupled with contrast matching, has emerged as a powerful tool to study lipid transport which, in addition, can track the movement of lipids in situ, removing the need to do step-wise sampling of the kinetic process.



2. Small angle neutron scattering (SANS) in the study of membranes

2.1 SANS nuts and bolts

SANS is an ideal technique to obtain structural information of particles, such as lipid vesicles and here we will briefly review the basics of SANS

to describe the strengths and advantages of this method (Mahieu & Gabel, 2018; Qian, Sharma, & Clifton, 2020). A careful and very detailed description of SANS, with an emphasis on biological systems, can be found in these references (Hamley, 2021; Sivia, 2011; Svergun, 2010; Svergun, Feĭgin, & Taylor, 1987).

In a small angle scattering experiment, a collimated incoming beam of neutrons—produced in nuclear reactors or in an accelerator-based spallation facility—impinge on a sample (typically in a 300 μ L quartz or other high neutron transmission cuvette) and the scattered neutrons are detected on a 2 dimensional ³He detector. Neutrons and other subatomic particles are characterized by a wavelength, λ , in the same way that X-rays, visible light, and other types of radiation are. For SANS, the neutron wavelength typically varies between 1 and 20 Å. The wave nature of the neutrons when scattered by nanoparticles ranging between 1 and 1000 nm results in an interference pattern that is then captured on a 2D detector. A schematic of the scattering process and the intensity pattern obtained from a solution of particles is shown in Fig. 1A.

The intensity pattern on the 2D detector for a random distribution of nanoparticles is radially symmetric and therefore can be radially averaged, as shown in the schematic in Fig. 1A. After being corrected by the empty sample container (quartz cell for example), sample transmission factor and incident neutron flux, an intensity versus Q curve in absolute scale (cm⁻¹) as shown in Fig. 1B is obtained. Q, as shown in Fig. 1A, corresponds to the magnitude of the neutrons' momentum direction change due to an elastic scattering event with the sample. In atomic units, Q is related to the scattering angle θ (see Fig. 1A) as follows:

$$Q = \frac{4\pi}{\lambda} \sin\left(\frac{\theta}{2}\right) \tag{1}$$

Since Q is inversely proportional to λ , it is inverselely porporional to length. Consequently, the larger length scales of the system, such as size and shape and overall composition, are captured in the low Q part of the spectra while smaller length scales such as the bilayer's structure and leaflet composition are captured in the higher Q range of the spectra (see Fig. 1B). Direct evaluation of the scattertered intensity pattern provides information on the particles' size and their inner structure as well as information relating to correlated distances between particles, typically found in concentrated solutions. The scattering intensity pattern however has significantly more detailed information which is retrieved through the use of models whose parameters

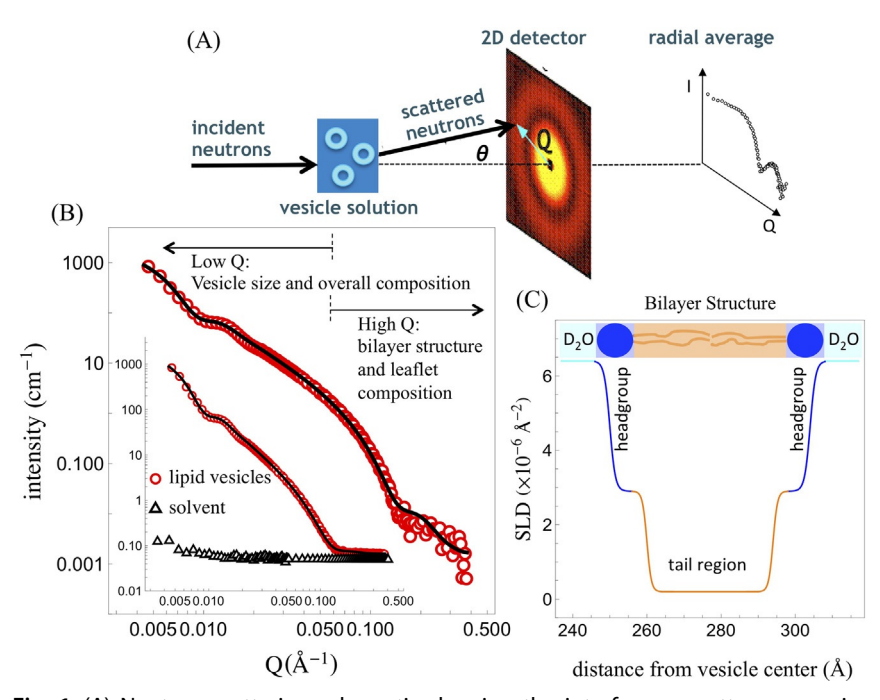


Fig. 1 (A) Neutron scattering schematic showing the interference pattern emerging from the scattering of neutrons by the sample, such as a solution of lipid vesicles, on a 2D detector which can be radially averaged if scattering is isotropic. (B) Scattering curve from unilamellar lipid vesicles, where the background has been removed and where the intensity, in the high Q (Q \sim 0.4/Å) has reached 10⁻³/cm. Hence, in this case, the data is reliable up to Q \sim 0.4/Å. Inset: Data before background subtraction. The near Q-independent solvent scattering, in this case D₂O, corresponds to the background signal. The line through the data corresponds to a fit for vesicles having a mean diameter of 50 nm—provided by the low Q—and inner structure corresponding to the headgroup and tail regions with distinct SLDs—provided by the high Q. (C) Scattering length density membrane profile corresponding to the fit shown in (B).

are optimized by fitting algorithms. Based on the best-fit values of these parameters, the experimenter makes conclusions about the nature of the scatterer.

In the simple case of a dilute solution of homogeneous particles, the intensity is given by:

$$I(Q) - I_{background} = \nu (SLD_{particle} - SLD_{solvent})^2 P(Q)_{particle}$$
 (2)

Here P(Q), the form factor, represents the model for the particles and contains the details of their shape and size. ν corresponds to the volume fraction of particles. The scattering length density, or SLD, corresponds to a measure

of the interaction of neutrons with the atomic and isotopic make-up of the particles and solvent. For example, at room temperature (\sim 20 °C), the SLD of H₂O is $-0.56 \times 10^{-6} \, \text{Å}^{-2}$, and of D₂O it is $6.37 \times 10^{-6} \, \text{Å}^{-2}$, corresponding to an order of magnitude difference in SLD values plus a sign reversal, while mixtures of H₂O and D₂O produce SLD values in between, given by a volume fraction relationship; for lipids (including lipid tails and headgroup), the SLD value is typically $0.2 \times 10^{-6} \, \text{Å}^{-2}$, but when hydrogens are replaced with deuteriums the SLD changes significantly, up to \sim 6.5 \times 10⁻⁶ Å⁻² when most hydrogens are replaced with deuteriums. Hence, the contrast term in Eq. (2), $SLD_{particle} - SLD_{solvent}$, can be exquisitely manipulated by the use of hydrogen to deuterium isotopes in the system, which makes the use of SANS so advantageous in the study of biological systems, where hydrogen (and therefore its substitution with deuterium) is abundant.

In Eq. (2) the particles are characterized by a single homogeneous SLD. In general, however, particles can certainly have inner structure, leading to regions with different SLDs. For example, lipid vesicles, depending on the contrast condition and on the experiment's Q-range and resolution, may reveal their inner structure: four onion-like layers corresponding to the two leaflets, each with a headgroup region and a tail region (as shown in Fig. 1C). In this case, Eq. (2) has to be modified to contain additional terms from these contributions.

In a system consisting of a solution of particles, such as vesicle dispersions in an aqueous solvent, the solvent background scattering, $I_{background}$, is nearly Q-independent as shown in the inset of Fig. 1B. When the $I_{background}$ is removed from the intensity, I(Q), the scattering signal can reach values as low as 10^{-3} /cm as shown in Fig. 1B, corresponding to attainable Q values typically between ~ 0.3 /Å and 0.4/Å. This Q range corresponds to a spatial resolution of ~ 10 Å. Although a scattering signal down to 10^{-4} /cm with reasonable statistics can be reached, it would take extremely long counting times and additional sample environment considerations which make it impractical in the typical beamtime awarded to use the instrument.

Although small angle scattering with X-rays (SAXS) has a higher flux than SANS and higher spatial resolution, the contrast variation tool-set available to SANS makes this the technique of choice in many contexts, particularly relating to direct measurement of membrane structures (e.g., membrane asymmetry (Liu et al., 2020; Nguyen et al., 2019) and/or domain formation (Heberle et al., 2013, 2016), or highlighting particular lipid species, like cholesterol (Garg et al., 2014, 2011). Still, SAXS and SANS

are certainly excellent complementary techniques when studying membrane structures in model lipid vesicles (Eicher et al., 2017; Heberle & Pabst, 2017) or in the complexity of cells (Semeraro, Devos, Porcar, Forsyth, & Narayanan, 2017; Semeraro, Marx, Frewein, & Pabst, 2021; Semeraro, Marx, Mandl, et al., 2021).

2.2 Contrast and contrast matching

As mentioned above, the difference in the scattering between hydrogen and deuterium makes SANS particularly powerful because it can straightforwardly reveal a specific process of interest or it can highlight a specific feature within a biological complex by eliminating the contribution from any other feature or process that is not the one of interest. Eliminating a particular signal is done through contrast matching which is a technique that is implemented straightforwardly. For example, if the scattering from the particles described by Eq. (2) is to be eliminated, the procedure consists on obtaining the solvent condition (a mixture of D₂O and H₂O) that brings the contrast term to 0 and produces an intensity that is flat and indistinguishable from the background scattering. To do this, one has to measure the scattering of the particles in solvents having several D₂O/H₂O ratios, and then, from a linear fit to the square root of the average low Q intensity minus the background vs the D₂O/H₂O ratio, we can obtain the zero intensity condition, known as the contrast match-point. Fig. 2 shows a schematic of vesicles in three different solvents, including the contrast match point as well as the contrast scattering series for deuterated POPC (1-palmitoyl-2-oleoyl phosphocholine) where the palmitoyl tail is fully deuterated (designated dPOPC). The scattering curves shown in the figure include the measurement of these vesicles in their contrast-matched (CM) solvent (48.6% D₂O), where indeed the corresponding scattering is flat as the solvent's SLD now matches the SLD of the vesicles. Fig. 2 also shows the linear fit to the square root of the background-subtracted low Q average intensity, from which the contrast matched point was determined. Then, from this invisible scaffold, any third component will then be revealed. For example, when studying cholesterol transport or cholesterol solubility in membranes, it is advantageous to eliminate the contribution from the phospholipids (Garg et al., 2014, 2011); in the studies of membrane proteins, it is advantageous to eliminate the contribution of the lipid scaffolding (Heinrich, Kienzle, Hoogerheide, & Losche, 2020; Johansen, Pedersen, Porcar, Martel, & Arleth, 2018); in the study of protein complexes,

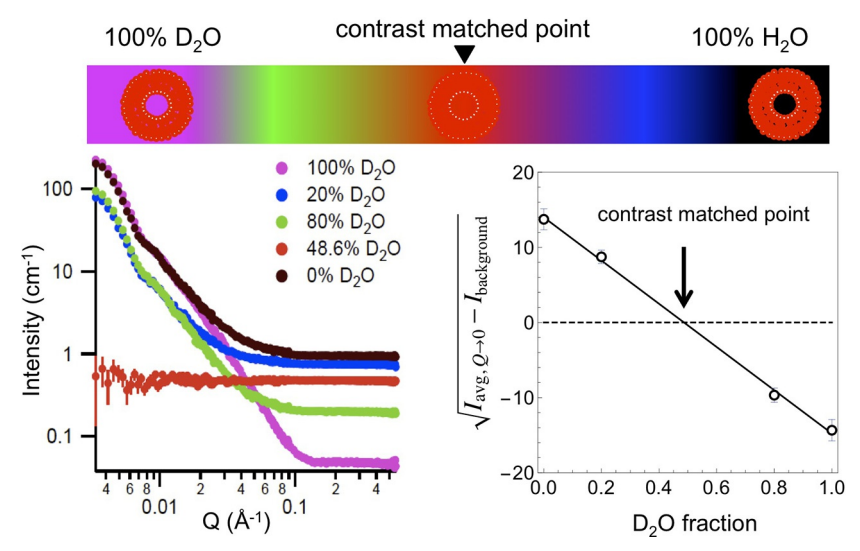


Fig. 2 Top: Schematic of vesicles in different solvent conditions. Lower Left: Scattering from dPOPC vesicles in five solvents: 100% D_2O , 80% D_2O , 48.6% D_2O (CM-point), 20% D_2O , 0% D_2O (100% H_2O). Lower Right: Square root of the average low Q intensity minus the background vs the D_2O/H_2O ratio. The contrast-matched (CM) point, corresponds to a 0.486 D_2O fraction from the linear fit, which indeed corresponds to fully CM vesicles as shown from the flat scattering in this solvent condition on the scattering plot shown on the left.

it is advantageous to obtain separate signals from distinct protein domains (Mahieu & Gabel, 2018; Sugiyama et al., 2014; Zaccai et al., 2016). This "highlighting" strategy has some parallel with ¹H NMR where the use of deuterium substitutions eliminate their peak contributions to the spectra. As has recently been highlighted, the diversity and complexity of the systems probed with neutrons, including membranes directly derived from cells, are dependent on our ability to deuterate selected parts of the system (Ashkar et al., 2018). This selective deuteration allows contrast conditions that highlight membranes in all their complexity, as shown recently by Nickels et al. in their study of nanoscale domains in the plasma membrane of gram-positive bacteria in vivo (Nickels et al., 2017). Although it is not necessarily trivial to perform high levels of deuterium substitutions, hydrogen is abundant in biological systems, and—to a lesser or greater extent, depending on the system's components—makes this approach possible. As such, in support of its user community, national neutron facilities have deuteration

initiatives to deuterate materials that are usually not available elsewhere, such as in the production of deuterated unsaturated lipids (Chakraborty et al., 2020; Darwish et al., 2013) and deuterated cholesterol (Moulin et al., 2018; Nickels et al., 2015).

Although deuteration does not change the chemical identity of lipids, deuteration does slightly affect their density and melting transition and can modify hydrogen bonding (Bryant et al., 2019; Luchini et al., 2018). The use of D₂O also affects the solubility of biomoleculaes compared to H₂O and modifies the solvent's pH (Efimova, Haemers, Wierczinski, Norde, & van Well, 2007). Indeed, D₂O has a significant effect on living organisms (Thomson, 1960). In spite of these effects, we have found that the transport properties of lipids appear not affected, as will be shown later in this chapter.

In this chapter, we will present work with lipids with all their hydrogens (also referred to as *hydrogenated* lipids) as well as lipids where selected hydrogens have been replaced with deuteriums, which we refer to as *deuterated* lipids. To highlight these differences, we use the letter h or d next to the lipid's acronym; for example, POPC is either hydrogenated, hPOPC or with 31 substituted deuteriums in the palmitoyl tail, dPOPC. Contrast matched points for the lipids used in the data presented in this chapter are: 13% D₂O for hPOPC, 48.6% D₂O for dPOPC, 56% D₂O for dPOPS (1-palmitoyl (d31)-2-oleoyl phosphoserine) and 87% D₂O for dDMPC (di-myristoyl (d54) phosphocholine) and 92% dDPPC (di-palmitoyl (d62) phosphocholine).

2.3 Time-resolved small angle neutron scattering (TR-SANS)

Time-resolved small angle neutron scattering has been successfully applied to the study of the transfer of lipids and sterols between and within membranes using unilamellar vesicles (Breidigan, Krzyzanowski, Liu, Porcar, & Perez-Salas, 2017; Garg et al., 2011; Nakano et al., 2007, 2009) and lipid nanodiscs (Nakano et al., 2009; Xia et al., 2015) by tracking structure and composition changes as a function of time. TR-SANS has also been used in the study of lipid exchange between vesicles and lipoproteins (Maric et al., 2019), and the transfer of lipids in the presence of transport modulators, which does not require any additional experimental design (Maric et al., 2019; Nakao, Kimura, Sakai, Ikeda, & Nakano, 2021; Nguyen et al., 2019, 2021; Nielsen, Bjørnestad, Pipich, Jenssen, & Lund, 2021; Nielsen, Prévost, Jenssen, & Lund, 2020). More recently, TR-SANS has been used

to exclusively study lipid flip-flop in vesicles with compositional asymmetry across membrane leaflets and changes in these kinetics due to protein interactions (Marx, Frewein, et al., 2021; Marx, Semeraro, et al., 2021; Nguyen, DiPasquale, Rickeard, Doktorova, et al., 2019). In addition to lipids and sterols, TR-SANS has been applied to other types of systems that exchange molecules such as the exchange of polymer chains between polymer micelles(Choi, Bates, & Lodge, 2011; Choi, Lodge, & Bates, 2010; Lund, Willner, Stellbrink, Lindner, & Richter, 2006).

The smallest temporal step with TR-SANS is in the subsecond range due to the relatively low number of neutrons produced at neutron facilities compared to the very large production of photons at X-ray facilities. More intense neutron sources are being planned or are under construction and they will certainly provide shorter time scales.

2.4 Measurement of the transfer of lipids and sterols between membranes using TR-SANS

To measure the transfer rate of a "probe" molecule of interest between membranes the approach is to have two vesicle populations, one enriched with the "probe" molecule, called donor vesicles, and the other devoid of the "probe" molecule, called acceptor vesicles. A schematic of possible contrast-matching schemes used to measure the transfer of one lipid species or a sterol between vesicles is shown in Fig. 3. At t=0, the two vesicle populations are mixed with "ideal" contrast conditions. For fast processes $(<\sim$ s), their capture requires the use of a stopped-flow apparatus (Cuevas Arenas et al., 2017) and a multitude of repeated experiments to obtain good statistics while for slow exchange, a single manual mixing is enough. Upon mixing, the exchange of the "probe" molecule between vesicles follows and is continuously tracked with TR-SANS until no more changes are detected in the scattering, indicating that the "probe" molecule is evenly distributed between all vesicles. TR-SANS directly detects the transport of the "probe" molecule from donor-to-acceptor vesicles without the need to physically separate donor from acceptor vesicles as other approaches have required, such as having to use centrifugation (Doktorova et al., 2018; Liu et al., 2020; Wimley & Thompson, 1991), filtration (Yancey et al., 1996), column separation (Dawoud & Abdou, 2021; McLean & Phillips, 1981), as well as other techniques (Sahoo et al., 2021).

The contrast scheme of Fig. 3 is not unique and certainly others are applicable too (Nakano et al., 2007; Wah et al., 2017). The advantage of the scheme shown in Fig. 3 is that it tracks a single species by removing

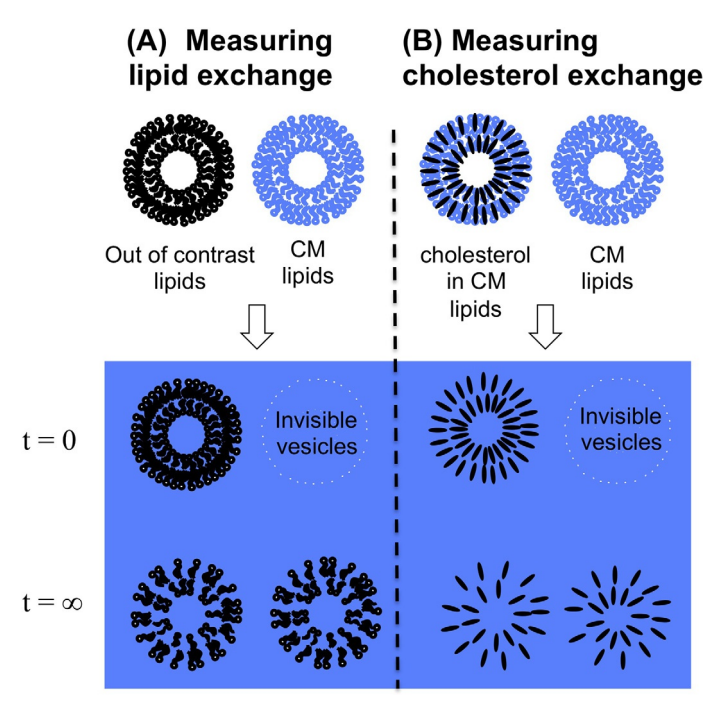


Fig. 3 Schematic of a scheme that focuses on highlighting one lipid species by contrast matching all other contributions. Therefore, the lipid species out of contrast is the only contribution to the scattering. (A) Schematic to highlight one lipid species while to other is CM. (B) Schematic to highlight cholesterol exchange in CM d-lipids.

the contribution of all other species in the system and therefore inarguably showing that changes in the scattering can only be due to the redistribution of that one species, such as was the case for cholesterol (Breidigan et al., 2017; Garg et al., 2011).

In the case of a dilute mixture of donor and acceptor vesicles, the scattering intensity has the contribution from both populations; following from Eq. (2) this is given by:

$$I(Q) - I_{incoh} = v_d (SLD_d - SLD_{solvent})^2 P(Q)_d + v_a (SLD_a - SLD_{solvent})^2 P(Q)_a.$$
(3)

Here, the subscripts d and a correspond to the donor and acceptor populations, respectively.

If the volume fraction of each population is the same and the vesicles are the same size, which is done by extruding the vesicles with the same filter size, the analysis of the experiment is simplified significantly. In this case, the changes in the scattering are only due to changes in composition in the vesicles, reflected in their SLDs. Hence Eq. (3) is simplified to:

$$I(Q,t) - I_{incoh} = \nu P(Q) \left(\left(SLD_d(t) - SLD_{solvent} \right)^2 + \left(SLD_a(t) - SLD_{solvent} \right)^2 \right) \tag{4}$$

The SLD of the vesicle can be obtained by averaging the SLD of the "probe" molecule (SLD_P) with that of the membrane $(SLD_{membrane})$ based on their corresponding volume fractions in the vesicle:

$$SLD_{d}(t) = \phi_{d}(t)SLD_{P} + (1 - \phi_{d}(t))SLD_{membrane}$$
 (5a)

$$SLD_a(t) = \phi_a(t)SLD_P + (1 - \phi_a(t))SLD_{membrane}$$
 (5b)

where $\phi_d(t)$ and $\phi_a(t)$ are the time-dependent volume fractions of the "probe" molecule in the donor and acceptor vesicles respectively, and where:

$$\phi_{\mathbf{a}}(\mathbf{t}) = \phi_{\mathbf{d}}(0) - \phi_{\mathbf{d}}(\mathbf{t}) \tag{6}$$

As mentioned earlier, the SLD of the solvent can be tuned by changing the D_2O/H_2O ratio and it can be set such that $SLD_{membrane} = SLD_{solvent}$ (as schematically shown in Fig. 3). In this case, the scattering intensity from the system is reduced to:

$$I(Q,t) - I_{incoh} = \nu P(Q) \left((\phi_d(t)\Delta SLD)^2 + ((\phi_d(0) - \phi_d(t))\Delta SLD)^2 \right)$$
(7)

where $\phi_d(0)$ is the initial volume fraction of the "probe" molecule in the donor vesicles and $\Delta SLD = SLD_P - SLD_{membrane}$. Hence, the final expression for the intensity is given by:

$$I(Q, t) = \beta(Q) \widetilde{I}(t.)$$

where $\beta(Q)$ is a time-independent prefactor corresponding to the scattering from the donor vesicles:

$$\beta(Q) = \nu \Delta \text{SLD}^2 \phi_J^2(0) P(Q) \tag{8}$$

while I(t) correspond to the compositional changes in the vesicles as a result of the transfer of only the "probe" molecule:

$$\widetilde{I}(t) = \varphi_d^2(t) + (1 - \varphi_d(t))^2$$
 (9)

Here, $\varphi_d(t) = \phi_d(t)/\phi_d(0)$. At t = 0, $\varphi_d = 1$ and thus $\widetilde{I} = 1$, which reflects that, initially, the acceptor vesicles are invisible to neutrons. At $t \to \infty$, $\varphi_d = 1/2$ which in turn results in $\tilde{I} = 1/2$, meaning that the overall scattered intensity drops by half at equilibrium when all vesicles have the same concentration of the "probe" molecule. Fig. 4A shows the initial and final scattering curves corresponding to the transfer of hPOPC in CM dPOPC vesicles as well as the transfer of dPOPC in CM hPOPC vesicles. The initial scattering curves change in intensity by half when they reach the equilibrium state since the donor-to-acceptor vesicles concentrations are the same. As shown in the plot, the acceptor vesicles were indeed CM since their scattering signal is flat. The signal from CM hPOPC vesicles is higher than the signal from CM dPOPC vesicles because of the higher content of hydrogen—coming mostly from H₂O. Hydrogen, in contrast to deuterium, produces a significantly higher background (for 48.6% D₂O it is 0.66/cm while for 13% D_2O it is $\sim 1/cm$). Also shown is a plot of the normalized intensity change due to the redistribution of hPOPC or dPOPC between the vesicles in the system. As expected, with a ratio of donors to acceptors of one, $\widetilde{I} = 1/2$ at equilibrium. Given that these curves overlap, we conclude that both hPOPC and dPOPC have the same transfer characteristics and that deuteration does not affect the transport mechanism. Fig. 4B shows the case of cholesterol transfer in CM dPOPC vesicles and the corresponding changes in the normalized intensity due to the redistribution of cholesterol between equal donor-to-acceptor vesicle populations. As with POPC transfer, at equilibrium $\tilde{I} = 1/2$.

If the ratio of donor-to-acceptor vesicles is not the same then Eqs. (8) and (9) have to be modified as follows:

$$\beta(Q) = \nu_d \Delta SLD^2 \phi_d^2(0) P(Q)$$
 (10a)

$$\widetilde{I}(t) = \varphi_d^2(t) + \frac{\nu_d}{\nu_d} \varphi_a^2(t) = \varphi_d^2(t) + \frac{\nu_d}{\nu_a} (1 - \varphi_d(t))^2$$
 (10b)

where,

$$\varphi_a(t) = \phi_a(t)/\phi_d(0) = \frac{v_d}{v_a}(1 - \varphi_d(t))$$
 (10c)

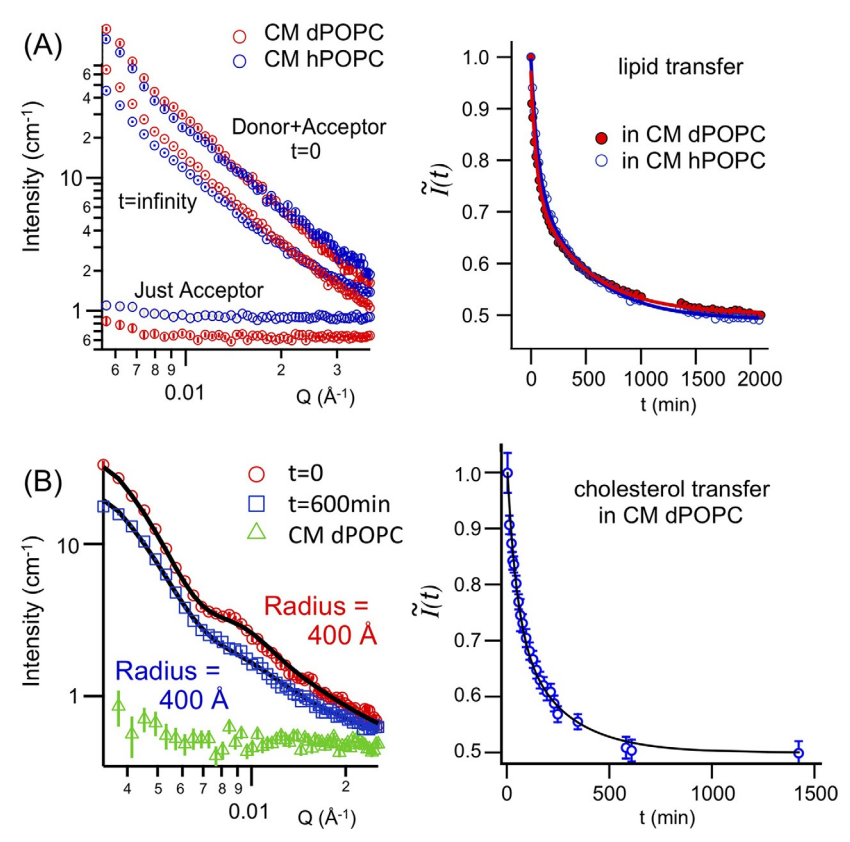


Fig. 4 (A) Left: Initial and final scattering from the transfer of hPOPC in CM dPOPC 100 nm in diameter vesicles as well as the transfer of dPOPC in CM hPOPC 100 nm in diameter vesicles at 75 °C. Scattering from CM acceptor vesicles is flat, with a higher overall signal from CM hPOPC vesicles due to the higher hydrogen content. TR-SANS data was acquired using a resolution that is not optimized to resolve structure but to obtain high flux and be able to track the changes over time with high statistics. Also, noteworthy, is that the compositional changes are captured in the low Q region of the spectra (Q_{max} < 0.04). Right: Normalized total intensity change due to the transfer of hPOPC between donor and acceptor vesicles as well as the transfer of dPOPC between donor and acceptor vesicles. The lines through the data are fits using first-order kinetic equations (Eqs. 12a-12d). Because these curves overlap, we conclude that deuteration does not affect the transport characteristics of POPC. The donor-toacceptor vesicles concentrations, being the same, shows an equilibrium value for the normalized total intensity of 0.5. (B) Left: t=0 and t=600 min scattering curves from the transfer of cholesterol in CM dPOPC at 50 °C. t=0, was measured without the acceptor vesicles and was used to normalize the total intensity as a function of time. The lines through the data correspond to fits using the vesicle form factor for a symmetric vesicle. Right: Normalized total intensity changes due to the transfer of cholesterol from donor-to-acceptor vesicles. The ratio of donor-to-acceptor vesicles is 1, and therefore, at equilibrium, the normalized intensity value is also 0.5. Lines through the data are a fit using Eqs. (12a)–(12d). Panel (B) left figure is reproduced from Garg, S., Porcar, L., Woodka, A. C., Butler, P. D., & Perez-Salas, U. (2011). Noninvasive neutron scattering measurements reveal slower cholesterol transport in model lipid membranes. Biophysical Journal, 101(2), 370-377. doi:10.1016/j.bpj.2011.06.014.

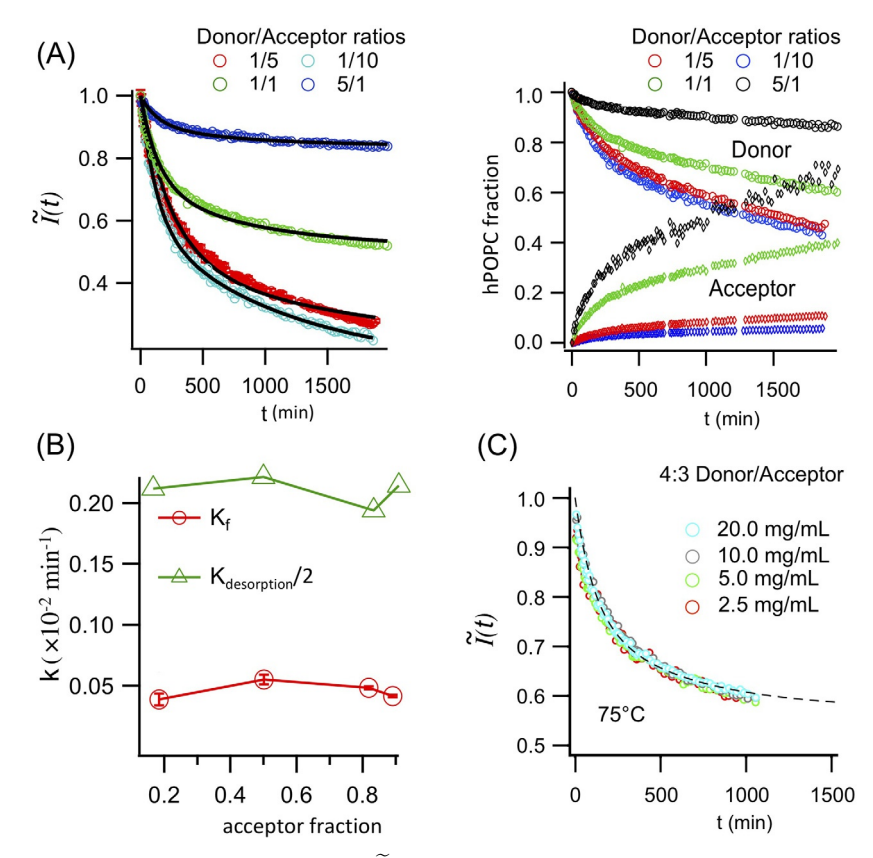


Fig. 5 (A) Left: Normalized intensity, $\widetilde{I}(t)$, for the transfer of hPOPC between donor and acceptor vesicles measured at constant total lipid concentration of 20 mg/mL, and where, initially, the acceptor vesicles are CM to the solvent. Shown are donor-to-acceptor ratios: 1:5, 1:1, 5:1 and 1:10. The kinetics were performed at 65 °C. The continuous lines correspond to fits to the data using Eqs. (12a)–(12d) and (13a)–(13c). Right: The fractions of hPOPC in donor and acceptor vesicles as a function of time derived from $\widetilde{I}(t)$ using Eqs. (10b) and (10c). (B) Respective rates for flip-flop and membrane desorption, k_f and $k_{desorption}$, obtained from the fits presented in (A). These rates are found to be independent of donor-to-acceptor ratio. (C) $\widetilde{I}(t)$ for 4:3 donor-to-acceptor ratio at 20, 10, 5 and 2.5 mg/mL highlighting free-diffusion of lipids rather than a transfer due to collisions (Jones & Thompson, 1989). The rates found from the fits (dashed line) are the same within the error bars: k_f =0.001±0.0001 min⁻¹ and $k_{desorption}/2$ =0.006±0.0002 min⁻¹. These data were taken at 75 °C.

Fig. 5A shows the normalized intensity, $\widetilde{I}(t)$, for the transfer of hPOPC between donor and acceptor vesicles having different population ratios. Because at equilibrium the "probe" is distributed evenly over all vesicles, with $\varphi_{d,a}(t=\infty) = \frac{\nu_d}{\nu_d + \nu_s}$, then, from Eq. (10b),

$$\widetilde{I}(t=\infty) = \frac{v_d^2}{(v_d + v_a)^2} + \frac{v_d v_a}{(v_d + v_a)^2} = \frac{v_d}{v_d + v_a}$$

Hence, when more acceptor vesicles are present than donor vesicles, the equilibrium intensity drops below ½, and when the number of donors dominates, the equilibrium intensity will be above ½, as shown in the figure. Indeed the equilibrium intensity is ½ when the ratio of donors to acceptors is 1:1.

As expressed by Eq. (10b), it is possible to obtain the overall composition changes in both the donor and acceptor vesicles directly from $\widetilde{I}(t)$. Fig. 5A also shows the corresponding compositional changes in donor and acceptor vesicles directly derived from $\widetilde{I}(t, \nu_d, \nu_a)$.

Although in this calculation we set $SLD_{membrane} = SLD_{solvent}$ following the scheme shown in Fig. 3, this is not a requirement and experiments can certainly be done using other contrast schemes (Nakano et al., 2007; Wah et al., 2017). For example, the use of the final equilibrium SLD of the vesicles may be the preferred solvent condition (Nakano et al., 2007; Nakao et al., 2021). The strength of the approach described in Fig. 3, however, is that the scattering comes only from the "probe" molecule with no other contribution, which is a procedure we used to track cholesterol (Breidigan et al., 2017; Garg et al., 2011) and shown in Fig. 4B. Indeed, if the simplifications used above are not valid then the new conditions have to be implemented starting with Eq. (3). Although the calculations may become more innvolved, the equation certainly still holds.



3. Kinetic and thermodynamic characteristics of the transport of lipids and sterols between and within membranes obtained from TR-SANS measurements

3.1 Obtaining transfer coefficients: Exchange and flip-flop of lipids and sterols in membranes

To extract the transfer coefficients from the scattering curves, we propose a simple first-order transfer between donor and acceptor vesicles as used previously (Garg et al., 2011). This model supposes that the transfer of the "probe" molecules originates from two types of pools: one pool resides in the outer leaflet of the membranes and is directly available to exchange with the outer leaflets of other membranes, while the other pool resides in the inner leaflet of the membrane which can only exchange with other vesicles

after it flips to the outer leaflet. If the intramembrane flipping rate is slow and hinders the intermembrane exchange rate, then both transfer contributions can be accessed by TR-SANS; otherwise, only the exchange process is captured. But how slow is "slow"? An analysis to this question was performed by Wah et al. (Wah et al., 2017) and found that in order to distinguish these two processes the flip-flop rate's upper limit has to be about 1.5 times the exchange rate. Currently the literature reports flop-flop events that range from minutes to days; however, the current technical limit is in the subsecond to seconds range with the use of a stop-flow apparatus and multiple measurements as mentioned earlier.

Let, C_{in_d} and C_{out_d} be the concentration of the "probe" molecule in the inner and outer leaflet of the donor population such that:

$$\varphi_d = C_{in \ d} + C_{out \ d} \tag{11a}$$

and

$$1 - \varphi_d = C_{in_a} + C_{out_a} \tag{11b}$$

where C_{in_a} and C_{out_a} are the concentration of the "probe" molecule in the inner and outer leaflet of the acceptor population. Then the time-varying concentration of the "probe" molecule in the leaflets of donor and acceptor vesicles is described by Eqs. (12a)–(12d):

$$\frac{dC(t)_{in_d}}{dt} = -k_f \left(C(t)_{in_d} - C(t)_{out_d} \right)$$
 (12a)

$$\frac{dC(t)_{out_d}}{dt} = k_f \left(C(t)_{in_d} - C(t)_{out_d} \right) - k_{ex} C(t)_{out_d} + k'_{ex} C(t)_{out_a}$$
 (12b)

$$\frac{dC(t)_{out_a}}{dt} = k_f \left(C(t)_{in_a} - C(t)_{out_a} \right) - k'_{ex} C(t)_{out_a} + k_{ex} C(t)_{out_d}$$
 (12c)

$$\frac{dC(t)_{in_a}}{dt} = -k_f \left(C(t)_{in_a} - C(t)_{out_a} \right)$$
 (12d)

where k_f corresponds to the rate coefficient for intraleaflet flip-flop, and where, k_{ex} and k_{ex}' correspond to the rate coefficients for exchange between the donor population and acceptor population.

If we assume the transfer of the "donor" molecules between vesicles happens through the aqueous phase via desorption from the bilayer (and where we also assume that the concentration of the "donor" molecule in the solvent is saturated and not changing in time) we find, as obtained by Jones et al. (Jones & Thompson, 1989), that the exchange rate, k_{ex} , is a function of the relative population of acceptors to donors and given by:

$$k_{ex} = \frac{\nu_a}{\nu_d + \nu_a} k_{desorption} \tag{13a}$$

where $k_{desorption}$ is the desorption rate from the bilayer into the aqueous phase. When $v_a = v_d$, the exchange rate is directly related the desorption rate:

$$k_{ex,\nu_d=\nu_a} = \frac{1}{2} k_{desorption} \tag{13b}$$

In addition, k_{ex} and k_{ex}' are related by:

$$k'_{ex} = \frac{v_d}{v_a} k_{ex} = \frac{v_d}{v_d + v_a} k_{desorption}$$
 (13c)

In Fig. 5A, the continuous lines through the data correspond to fits to $\widetilde{I}(t)$ using the kinetic model described by Eqs. (12a)–(12d) and (13a)–(13c). From the fits we obtained the rates for lipid desorption, $k_{desorption}$, and for lipid flip-flop, k_f . As shown in Fig. 5B, these rates are independent of the donor-to-acceptor ratio, as expected.

When flip-flop is not rate-limiting to the exchange process, Eqs. (12a)–(12d) reduce to:

$$\frac{d\varphi_d(t)}{dt} = -\frac{k_{ex}}{2}\varphi_d(t) + \frac{k'_{ex}}{2}(1 - \varphi_d(t))$$
 (14)

where the exchange coefficients are given by Eqs. (13a)-(13c).

A comparison between the case where we consider flip-flop between inner and outer leaflets as rate-limiting to the exchange process (Eqs. 12a–12d) and the case where we only consider an exchange process (Eq. 14) is shown in Fig. 6. The plot on the left corresponds to the transfer of hPOPC in CM dPOPC vesicles, while the plot on the right corresponds to the transfer of cholesterol in CM dPOPC vesicles. This experimental scheme (schematically outlined in Fig. 3) assures that the intensity changes are only due to hPOPC or cholesterol transferring between donor and acceptor vesicles. As shown, we clearly find that the model where flipping is limiting the exchange process is the one that best describes both data sets (Garg, Porcar, Woodka, Butler, & Perez-Salas, 2012).

In the case where the transfer does not primarily happen through the aqueous phase, but through vesicle collisions, Jones et al. propose an effective concentration-dependent exchange rate (Jones & Thompson, 1989). Fig. 5C shows the normalized intensity changes for the transfer of

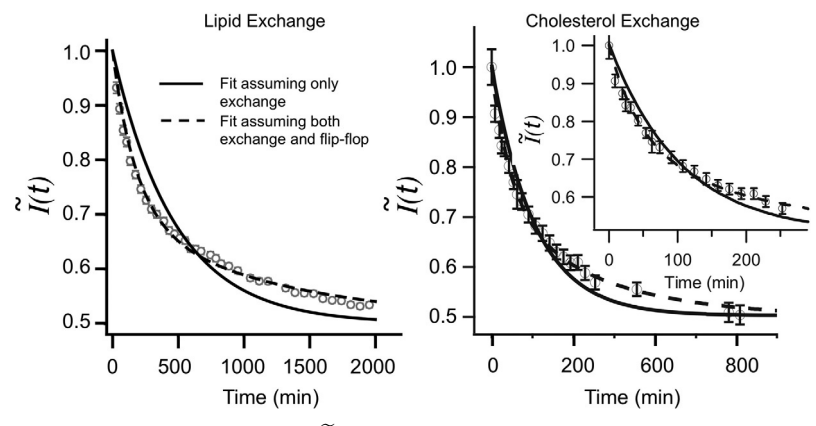


Fig. 6 Normalized total intensity, I(t), for the transfer of hPOPC (left) and cholesterol (right) in CM 100 nm in diameter dPOPC vesicles having a 1:1 donor-to-acceptor ratio. The lines through the data compare the case where flip-flop between leaflets is rate limiting to the exchange process and the case when it is not (hence we only detect exchange). The model where flipping is limiting the exchange process (dashed line) is the one that best describes both data sets. Inset: a close-up on the kinetic intensity change at short times for the case of cholesterol exchange. Figure on the right is reproduced from Garg, S., L. Porcar, A. C. Woodka, P. D. Butler, and U. Perez-Salas. (2012). Response to "how slow is the Transbilayer diffusion (Flip-flop) of cholesterol? Biophysical Journal, 102(4), 947–949.

hPOPC between CM dPOPC vesicles having a 4:3 donor-to-acceptor population ratio at four concentrations, 2.5, 5, 10 and 20 mg/mL. The data, as well as the fits, show that there are no perceptible concentration-dependent effects.

If we take a closer look at the schematic in Fig. 3, there is a fundamental difference between the two experiments. In Fig. 3A, for the case of lipids, there is no mass exchange—the exchange is isotopic—while in Fig. 3B, which is the case of cholesterol, the transfer is driven by a redistribution of mass. In the case of mass transfer, such asymmetry in the composition of the vesicles could generate a driving force to equilibrate the chemical potential such that the exchange becomes faster than in the isotopic exchange case. Fig. 7 compares the two cases. In one case, we studied the isotopic exchange of 35 mol% of h and d DMPC in CM dDPPC vesicles while in the other case we studied the redistribution of 35 mol% hDMPC between CM dDPPC vesicles. We find that the isotope exchange is captured quite accurately by Eqs. (12a)—(12d). In the case of mass transfer, while the fit is not as good, the model captures the overall behavior of the data

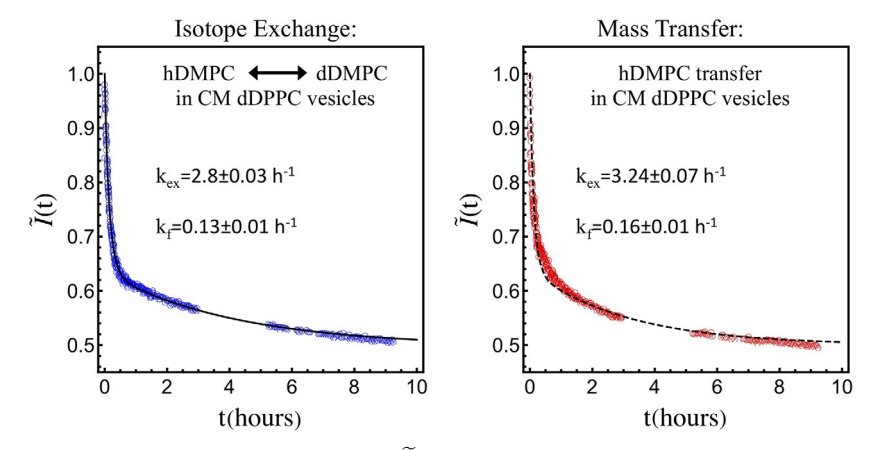


Fig. 7 Normalized total intensity, I(t), for, left, isotopic transfer: hDMPC +dDPPC \Leftrightarrow dDMPC+dDPPC and, right, mass transfer: hDMPC+dDPPC \Leftrightarrow dDPPC. The concentration of hDMPC in the donor vesicles was 35 mol%. The concentration of dDMPC in the acceptor vesicles, in the case of the isotope exchange experiment, was also 35 mol%. The temperature was set to 65 °C. The lines through the data correspond to fits using the exchange and flipping model (Eqs. 12a–12d).

and both fits produce rates that differ by only factors of order 1 as shown in the figure. Hence, in this case, mass transfer is having a negligible effect on the rates of transfer.

3.2 Obtaining the energetics of lipid and sterol transport

The rate constants measured are temperature dependent, increasing with increasing temperature and generally following an Arrhenius behavior. This behavior establishes a linear relation between the natural logarithm of the rates and the inverse of the absolute temperature. Fig. 8A shows the temperature dependent $\tilde{I}(t,T)$ for the transfer of hPOPC in CM dPOPC membranes as well as the transfer of cholesterol in CM dPOPC membranes. Fig. 8B shows the corresponding Arrhenius plot for the transfer rate coefficients, flipping and exchange for both cholesterol (red) and hPOPC (blue). The activation energy, E_a , for flipping and for exchange is obtained from the slope in the Arrhenius plot. In addition to the activation energy, it is possible to extract thermodynamic parameters according to Eyring's transition state theory (Eyring, 1935; Laidler & King, 1983) through the implementation by Homan et al. (Homan & Pownall, 1988) where the activation entropy, ΔS^{\ddagger} , and the activation enthalpy, ΔH^{\ddagger} , are related as follows:

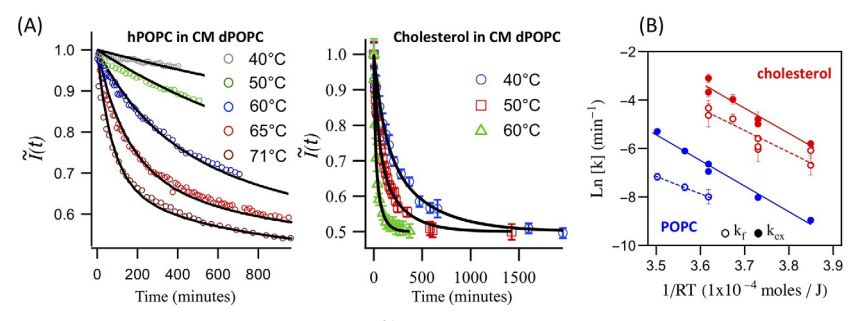


Fig. 8 (A) Normalized total intensity, $\tilde{I}(t,T)$, for the transfer of hPOPC in CM dPOPC vesicles (left) and cholesterol transfer in CM dPOPC vesicles (right) as a function of temperature. Lines through the data correspond to fits using Eqs. (12a)–(12d). (B) Arrhenius plot for the rates of exchange and flip-flop for cholesterol (red) and hPOPC (blue) in dPOPC CM vesicles obtained from the fits shown in (A) as a function of temperature. Open symbols correspond to flip-flop rates and solid symbols correspond to exchange rates. Cholesterol data reproduced from Garg, S., Porcar, L., Woodka, A. C., Butler, P. D., & Perez-Salas, U. (2011). Noninvasive neutron scattering measurements reveal slower cholesterol transport in model lipid membranes. Biophysical Journal, 101(2), 370–377. doi:10.1016/j.bpj.2011.06.014.

$$e^{\Delta S^{\ddagger}/R} = \frac{N_A h}{RT} \kappa_{T^*} e^{-\Delta H^{\ddagger}/RT} \tag{15}$$

where N_A , h, R are Avogadro's number, Plank's constant and the gas constant, respectively. T is temperature in Kelvins and κ_{T^*} corresponds to the rate extrapolated to 37 °C (in absolute temperature, 310 K). The activation enthalpy is related to the activation energy as follows $\Delta H^{\ddagger} = E_a - RT$ and the difference between the activation enthalpy and the activation entropy term $T\Delta S^{\ddagger}$ is the activation free energy: $\Delta G^{\ddagger} = \Delta H^{\ddagger} - T\Delta S^{\ddagger}$.

Table 1 shows the corresponding thermodynamic values obtained through this analysis for hPOPC as well as for cholesterol transfer, flip-flop and exchange, in CM dPOPC vesicles. Although we will discuss in more detail these results in the section below, we can make the following observations. We find that the rates for exchange and flip-flop for POPC and the energetics for these processes are consistent with values found in the literature. However, for cholesterol, the results shown in Fig. 8 and Table 1 are surprising. Fig. 8B shows that the exchange and flip-flop rates of POPC are about 20 times slower than those found for cholesterol, but cholesterol is found to flip-flop surprisingly slow too, taking many hours at physiological temperatures. We also find that the energetics for cholesterol exchange is similar to those of POPC. This is perhaps not too surprising

ut 37 C.	K (h ⁻¹)	T1/2 (h)	Ea (KJ)	$\Delta \text{H}^{\ddagger}(\text{KJ})$	$T\DeltaS^{\ddagger}(KJ)$	$\Delta G^{\dagger}(KJ)$
	POPC					
Flipping	0.0029 ± 0.0001	234 ± 1	72 ± 2	69±2	43 ± 2	112±1
Exchange	0.0040 ± 0.0001	158 ± 1	106 ± 7	103 ± 7	8 ± 7	111±5
	Cholesterol					
Flipping	0.05 ± 0.03	13 ± 3.7	90 ± 14	88 ± 14	17 ± 14	105 ± 10
Exchange	0.09 ± 0.02	8.5 ± 0.3	104 ± 5	101 ± 5	2±5	104 ± 3

Table 1 Thermodynamic parameters for cholesterol and POPC exchange and flipping at $37\,^{\circ}$ C.

knowing the location of cholesterol in the membrane (Waldie et al., 2019). On the other hand, the energetics for flipping is slightly lower for cholesterol, which can be understood in terms of its smaller hydrophilic volume.



4. Transport behavior of lipids and sterols in membranes

4.1 Exchange and flip-flop behavior of lipids in model membranes

The passive exchange of lipids between membranes and flip-flop within membranes has been demonstrated to be slow. But it is also because lipids move slowly that lipid gradients between different membranes and within membranes can be established. The structural characteristics of lipids, imparting in them slow transport through an aqueous environment as well as between membrane leaflets, allows for some passive regulation mechanism to maintain composition gradients without having, potentially, a significant contribution from ATP-dependent mechanisms to maintain them.

Tail structure, tail length as well as lipid headgroup type determine the time-scale of this passive regulation. Using TR-SANS, we have started to quantify lipid transport characteristics and passive energetic landscapes. We found, that DMPC (dimyristoyl phosphocholine), which is a two tail 14 carbon (C14) long saturated phosphocholine lipid, exchanges and flip-flops in DMPC membranes faster than in DPPC (dipalmitoyl phosphocholine) membranes, where DPPC is a two tail 16 carbon (C16) long saturated phosphocholine lipid. Although this is an expected trend, it was interestingly to find that it is the membrane thickness (a change of ~8 Å (Kucerka, Nieh, & Katsaras, 2011)) that produces the largest effect.

Flipping and exchange transport rates for DMPC in DMPC membranes at 65°C can be extracted from the thermodynamic parameters reported by Nakano et al. (Nakano et al., 2007), and giving a flip-flop rate of 0.63 h⁻¹ and an exchange rate of 4.2 h⁻¹. Comparing to the values found in DPPC membranes (Fig. 7) we see a slowdown by a factor of ~4 for flipping and ~ 1.3 for exchange. It is not too surprising to find roughly the same value for the exchange of DMPC between DMPC and DPPC (C14 vs C16). However, for flipping, it is clear that DMPC will necessitate more energy to flip inside a thicker bilayer. DPPC flip-flop in DPPC membranes at 65 °C, on the other hand, was found to be $0.03\,\mathrm{h^{-1}}$ by Marquardt et al. (Marquardt et al., 2017) using ¹H NMR, which is roughly a factor of 5 slower than DMPC in DPPC membranes. NMR is an alternative technique that can be used to measure lipid flip flop in vesicles. We recently found that in the case of DPPC, flip flop rates measured by ¹H NMR and SANS were consistent (Liu et al., 2020). Hence, both the hydrophobic volume of the molecule that flips and the host membrane thickness are important determinants in the flip-flop rates.

Another important potential factor affecting the rates is the tail structure. DPPC and POPC membranes have a similar thickness (within ~1 Å (Kucerka et al., 2011)), however, POPC has one 18 carbon long monounsaturated tail and a second C16 saturated tail. From Table 1, we see that POPC flips in POPC membranes at a rate of 0.03 h⁻¹ at 65 °C, which is the same flip-flop rate for DPPC in DPPC at 65 °C. Perhaps surprising is that the differences in the tail order between these two lipids (Seelig & Seelig, 1977) is not showing a difference in the flip-flop rate in this case. Hence, the dominant effect for flipping is a correlation between membrane thickness and the tail length of the lipid "probe."

Although in this case we do not have the exchange rate of DPPC between DPPC membranes we anticipate them to be similar to those of POPC because they have similar tail lengths and have the same headgroup. Comparing the exchange rate of DMPC in both C14 and C16 and the exchange rate of POPC between POPC membranes at 65 °C we find that POPC exchanges about 30 times slower than DMPC.

In addition to the rates, we find that the thermodynamic parameters for lipid exchange and flip flop obtained from TR-SANS measurements for DMPC by Nakano et al. (Nakano et al., 2007) and for POPC (as shown above) show similar trends: the activation energy to flip is slightly lower than to exchange (by \sim 20 to 30 kJ/mol) while the corresponding free energies are slightly lower for DMPC (around 100 kJ/mol) than for POPC (around 110–115 kJ/mol).

These trends were also captured by MD simulations (Sapay, Bennett, & Tieleman, 2009). The simulations show that the energy barrier for lipids to desorb from the membrane into the aqueous medium and the energy barrier to flip across the bilayer center are similar and increase with bilayer thickness. Interestingly, Sapay et al. also find that these energy barriers in membranes that have similar bilayer thickness but different saturation (for example, DPPC vs POPC) are nearly identical. A quantitative comparison between the free energies obtained by the simulations and TR-SANS, however, show that the free energies in the simulations are lower than what is obtained in TR-SANS experiments. In the case of POPC, the difference is not large, with simulations predicting an energy barrier of ~95 kJ for both lipid desorption from the membrane and lipid flip-flop. In the case of DMPC the difference is a factor of more than 2, with simulations predicting a value of 40 kJ/mol.

Although membrane order (between POPC and DPPC) has no detectable effect on lipid flip-flop, as discussed above, Nakano et al. (Nakano, Fukuda, Kudo, Matsuzaki, et al., 2009) showed that membrane order induced by cholesterol has a significant effect. Using TR-SANS Nakano et al. showed that DMPC membranes with cholesterol can slow down the flip-flop rates of DMPC significantly; at 40 mol%, the highest concentration of cholesterol studied, the flip-flop rate of DMPC had decreased by a factor of at least ~20, while at 20 mol% the flip-flop rate had only slowed down by a factor of ~4. Yet the exchange of DMPC between membranes remained unaffected.

MD simulations studying the process of flip-flop of lipids in the presence of cholesterol show similar trends overall (Bennett, MacCallum, & Tieleman, 2009). The study, using DPPC, finds that the energy barrier to flip increases at the bilayer center, from ~75 kJ/mol with no cholesterol to ~115 kJ mol with 40 mol% cholesterol. The simulations, however, also predict a lowering of the energy barrier to desorb from the bilayer with the addition of cholesterol, which is not detected in the experiments.

In addition to tail variations through saturation state and length, lipids also have different headgroup types, particularly in regard to charge. POPS, POPG (1-palmitoyl-2-oleoyl-sn-glycero-3-phosphoglycerol) and POPA (1-palmitoyl-2-oleoyl-sn-glycero-3-phosphate), for example, have the same tail structure as POPC, but the headgroups are negatively charged. POPS, POPG and POPA are important signaling lipids and their distribution in cellular mambranes is specific (van Meer et al., 2008); for example, POPS is found primarily in the inner leaflet of the PM, while POPC,

and saturated lipids, are found mostly in the outer leaflet of the PM. In their study of POPA (Nakano, Fukuda, Kudo, Matsuzaki, et al., 2009) and POPG (Nakano, 2019), Nakano and colleagues find that the smaller headgroups in these lipids, though charged, produce a slower intervesicluar exchange and in particular faster flip-flop rates, which at 37 °C correspond to halftimes between 420 and 230 min, while for POPC, as shown in Table 1, it takes hundreds of hours. Fig. 9 supports this observation, where POPS, having a similar size headgroup to POPC, has similar exchange and flip-flop rates to those of POPC, varying by less than a factor of 2.

Experimentally, we have also investigated the effect of membrane curvature on the transfer rates (potentially being another source of discrepancy) by comparing the transport of DMPC using 100 nm vesicles and 30 nm vesicles. We found that the rates increase slightly when increasing the curvature of the vesicles, ie, we find faster rates in 30 nm vesicles compared to 100 nm vesicles. The effect, however, is of order ~1. On the other hand, the energetics for both flip-flop and exchange remain essentially the same (Wah et al., 2017). Recent MD simulations find a similar result, where the energetics of lipid flip-flop and lipid desorption are found to be independent of curvature (Jing, Wang, Desai, Ramamurthi, & Das, 2020).

Certainly, the feedback loop between experiments and MD simulations will ultimately reveal an ever more detailed molecular picture underlying various structural and dynamic processes in membranes.

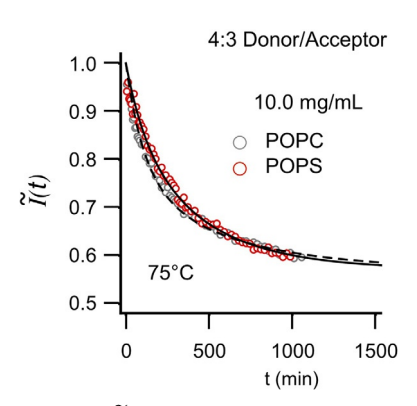


Fig. 9 Normalized total intensity, I(t), for the transfer of hPOPC in CM dPOPC vesicles and hPOPS in CM dPOPS vesicles at $T=75\,^{\circ}$ C. The lines through the data correspond to fits using Eqs. (12a)–(12d). The rates found were for POPC: $k_f=0.001\pm0.0001\,\mathrm{min}^{-1}$ and $k_{desorption}/2=0.006\pm0.0002\,\mathrm{min}^{-1}$, and for POPS: $k_f=0.0018\pm0.0001\,\mathrm{min}^{-1}$ and $k_{desorption}/2=0.0043\pm0.0002\,\mathrm{min}^{-1}$.

4.2 Exchange and flip-flop behavior of sterols in model membranes

4.2.1 Cholesterol transfer

Cholesterol is the most abundant lipid of the PM with a 2:1 ratio to the total amount of lipids (Kobayashi & Menon, 2018). Currently, existing evidence on cholesterol's distribution in the PM spans almost the entire range of possible outcomes, from mostly residing in the inner leaflet (Courtney et al., 2018; Mondal, Mesmin, Mukherjee, & Maxfield, 2009; Solanko et al., 2018) to more than 10-fold enrichment in the outer leaflet (Buwaneka, Ralko, Liu, & Cho, 2021; Liu et al., 2017). Therefore, there is significant debate concerning possible biases in understanding these conflicting results. This highlights the challenges of measuring the leaflet occupancy of this molecule (Steck & Lange, 2018). Cholesterol, in contrast to lipids, is seen as a molecule that can traverse the lipid bilayer much faster than lipids (Bruckner et al., 2009; Hamilton, 2003; London, 2019; Steck et al., 2002). Simulations support this result as well (Atkovska, Klingler, Oberwinkler, Keller, & Hub, 2018; Baral et al., 2020; Bennett, MacCallum, Hinner, et al., 2009; Bennett & Tieleman, 2012; Gu et al., 2019). Therefore in order to produce an asymmetric distribution of cholesterol in the PM other mechanisms—yet to be identified—have to play a significant role (Doktorova, Symons, & Levental, 2020).

Our TR-SANS findings suggest that one mechanism facilitating this is, as with lipids, a spassive regulation strategy: if flips slowly (Breidigan et al., 2017; Garg et al., 2011). As shown in Table 1, the flip-flop and exchange rates for cholesterol in POPC membranes are an order of magnitude faster than those for POPC in POPC membranes. In contrast, the corresponding energies of activation and free energy barriers for flip-flop and for exchange between membranes are similar. MD simulations do show that cholesterol's free energy barrier to desorb from the lipid bilayer into the aqueous environment is similar to lipids, such as DPPC and POPC. However, cholesterol's free energy barrier to flip is found to be significantly lower, by factors between 3 and 10 (Bennett, MacCallum, Hinner, et al., 2009; Sapay et al., 2009). One hypothesis we proposed for this inconsistency between TR-SANS and MD simulations was a possible issue with the force fields used to describe cholesterol. For example, using coarse grain MD simulations and the MARTINI force field, we found that the amount of cholesterol incorporated into membranes was overestimated; the simulations would put cholesterol molecules at the bilayer's center rather than expelling these molecules from the membrane altogether (Garg et al., 2014).

In terms of experimental biases, these include the use of analogs (Garg et al., 2011; Nyholm, Jaikishan, Engberg, Hautala, & Slotte, 2019), or the use of extraneous molecules like cyclodextrin (Garg et al., 2011). A bias in the work by Bruckner et al. (Bruckner et al., 2009) using ¹³C NMR and labeled ¹³C cholesterol is not obvious. Their work shows very fast flip-flop (ms range) for cholesterol. A possible bias in our TR-SANS measurements were brought up by Kelley et al., who have pointed out that unilamellarity in vesicles between 30 and 100 nm is not always reached and is actually better attained when using at least a small amount of charged lipids (~1–5%) (Scott et al., 2019). Fig. 10 shows a plot for the transfer of cholesterol between CM 50 nm in diameter dPOPC vesicles having 3 mol% of charged lipids at 50 °C where found that the flip-flop and exchange rates are the same as those in Garg et al. (Garg et al., 2011)

Other factors affecting the transfer rates are possible differences in the state of cholesterol within the membrane, such as whether a higher concentration of cholesterol will slow down the process because of synergetic or collaborative motions. Fig. 10 shows that cholesterol concentration effects depend on the lipid environment; we find that while in POPC the change

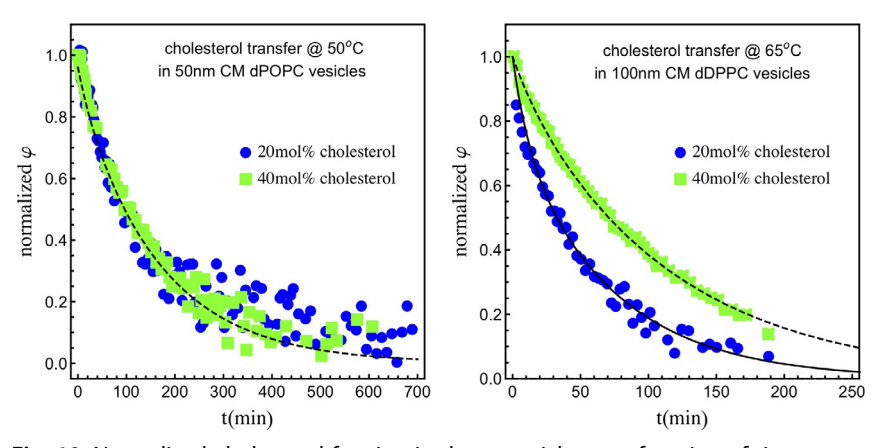


Fig. 10 Normalized cholesterol fraction in donor vesicles as a function of time at two different cholesterol concentrations: 20 and 40 mol%. Left plot, at 50 °C in 50 nm in diameter CM dPOPC vesicles with 3 mol% dPOPG (1-palmitoyl (d31)-2-oleoyl-phosphoglycerol). Right plot, at 65 °C in 100 nm in diameter CM dDPPC vesicles with 2 mol% dDPPG (dipalmitoyl (d62)-phosphoglycerol). Lines through the data correspond to fits with Eqs. (11a)–(11b) and (12a)–(12d). The rates for cholesterol in 50 nm POPC vesicles at 50 °C are, k_f =0.01 \pm 0.004 min⁻¹ and $k_{desorption}/2$ =0.008 \pm 0.0005 min⁻¹. The rates for cholesterol in 100 nm DPPC vesicles at 65 °C are k_f =0.02 \pm 0.004 min⁻¹ and $k_{desorption}/2$ =0.03 \pm 0.002 min⁻¹ at 20 mol% cholesterol, and k_f =0.02 \pm 0.004 min⁻¹ and $k_{desorption}/2$ =0.01 \pm 0.002 min⁻¹ at 40 mol% cholesterol.

in cholesterol concentration from 20 mol% to 40 mol% has no effect on the transport of cholesterol, in DPPC, a saturated lipid, there is. Fits to the normalized intensity (or normalized cholesterol fraction, as shown in the figure) with Eqs. (12a)–(12d) suggest that flip-flop is unaffected by cholesterol concentration but that the exchange rate decreases by a factor of nearly ~3. Comparing the transfer rates of cholesterol between POPC and DPPC in Fig. 10 as well as when varying the ratio of saturated to monounsaturated tails, as shown in Fig. 11A (taken from Breidigan et al. (Breidigan et al., 2017)), we find that the rates for cholesterol increase gradually, by at most a factor of 6, as the fraction of unsaturated tails increase from all DPPC membranes to all POPC membranes. One prediction found by MD simulations that we did not observe in our measurements was a significant slowdown of cholesterol flip-flop rates due to a "raft" effect (a raft being a mixture of sphingomyelin, POPC and cholesterol). In the simulations of a raft mixture, done at 50 °C, cholesterol's flip-flop halftimes increased several orders of magnitude to ~30min in contrast to milliseconds found in non-raft mixtures. Our measurement of a raft-like system did not slowdown cholesterol's flip flop dramatically; instead the lifetimes (rates) were found to be similar to those in non-raft mixtures as shown in Fig. 11A (Breidigan et al., 2017).

In deciphering cholesterol's location in the cell, we start by noting that the lipid environment across organelle membranes is very different (van Meer et al., 2008). This difference could certainly have an impact on cholesterol transfer and can hold clues as to what may drive cholesterol to one particular environment over the other. Shown in Fig. 11B, are cholesterol's exchange kinetics in POPC and POPS. We find that the rates are not only an order of magnitude slower in POPS than in POPC at near physiological temperatures, but that they exhibit a surprising discontinuous Arrhenius behavior around 48 °C, where cholesterol appears nearly frozen at physiological temperatures. In this case, flip-flop kinetics were not rate limiting and therefore not captured in these measurements. The thermodynamic analysis showed that at biologically relevant temperatures, below the discontinuity, the exchange of cholesterol is entropically dominated while it is enthalpically driven, as is the case in POPC vesicles, above that discontinuity. In this case, the use of Laurdan (see chapter "Evaluating membrane structure by Laurdan imaging: Disruption of lipid packing by oxidized lipids" by Levitan in this volume) provided additional information, pointing to a quasi order-disorder transition in the headgroup region responsible for this effect, even while the lipid tail environment was in the fluid phase.

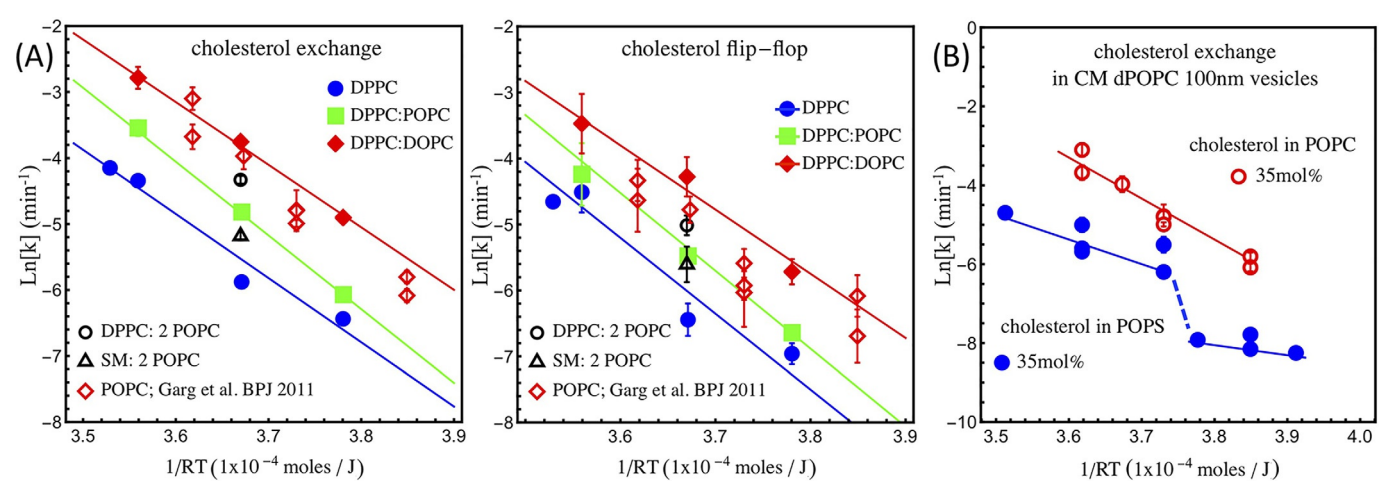


Fig. 11 (A) Arrhenius plots comparing the exchange and flip-flop rates in different membrane environments, where the fraction of saturated lipids is varied relative to the unsaturated lipid fraction. We observe a transfer slowdown with an increase in chain saturation in the membrane. Surprisingly though, the energetics for exchange and flip-flop remains the same as can be assessed from the near parallel Arrhenius behavior. (B) Arrhenius plot comparing the exchange of cholesterol in POPC vesicles to the exchange of cholesterol in POPS vesicles. We find an unusual (anomalous) transition, where the exchange becomes nearly frozen for temperatures below 48 °C. Panel (A) is reproduced from Breidigan, J. M., Krzyzanowski, N., Liu, Y., Porcar, L., & Perez-Salas, U. (2017). Influence of the membrane environment on cholesterol transfer. Journal of Lipid Research, 58(12), 2255–2263. doi:10.1194/jlr.M077909. Panel (B) is reproduced from S. Garg, S., Liu, Y., Perez-Salas, U., Porcar, L., & Butler, P. D. (2019). Anomalous inter-membrane cholesterol transport in fluid phase phosphoserine vesicles driven by headgroup ordered to disordered entropic transition. Chemistry and Physics of Lipids, 223, 104779. doi:10.1016/j.chemphyslip.2019.05.004.

This surprising result also triggered research on cholesterol's solubility in POPS membranes. The strength of SANS to study how much cholesterol can be incorporated into membranes comes from our ability to matchout the lipids, and therefore only highlighting cholesterol. Using this approach, we verified that cholesterol can incorporate in POPC membranes up to 61 mol% as previously shown (Huang, Buboltz, & Feigenson, 1999; Stevens, Honerkamp-Smith, & Keller, 2010), while in POPS it was found to be unexpectedly high, 73 mol% (Garg et al., 2014). The consequences of these findings are still being investigated. However, as discussed in Garg et al. (Garg et al., 2014), this finding suggests that a higher than physiologically relevant cholesterol concentration in the PM is not driven to form toxic cholesterol crystals due to the presence of POPS.

4.2.2 Sterol structure effects on transfer

In addition to the effects that the lipid environment has on the transfer rates of cholesterol, we have also investigated the effect of structural changes to the cholesterol molecule to identify correlations between structure and transport properties. Fig. 12A shows the effect of adding double bonds on the steroid ring and its tail—dehydroergosterol (DHE)—while Fig. 12B shows the effect of the replacement of the hydroxyl group by a sulfate group. These sterols have physiological and even beneficial functions; for example, DHE has been found to be help treat cognitive function loss (Ano & Nakayama, 2018) while cholesterol sulfate, which is a component of cell membranes, aids in protecting erythrocytes from osmotic lysis as well as in regulating sperm capacitation (Strott & Higashi, 2003). As shown in the figure, the increase in double bonds in the ring structure as well as the tail in DHE, increases the transport properties dramatically; DHE exchanges 8 times faster and flips 10 times faster than cholesterol (Garg et al., 2011). This is an interesting results since DHE has been found to be asymmetrically distributed in the PM of CHO (Mondal et al., 2009), yeast (Solanko et al., 2018) and synaptic (Wood, Igbavboa, Muller, & Eckert, 2011) cells, which suggests that even though we found that this sterol moves very fast through the lipid bilayer, the lipid and protein compositional asymmetry in combination with sterol transport proteins in the PM, are likely keeping DHE in the cytoplasmic leaflet. The presence of the sulfate moiety in cholesterol sulfate produces a fast transfer through the solvent, shown in the precipitous drop in the normalized total intensity. The value of 0.625 for the normalized intensity, as given by Eq. (9), corresponds exactly to the outer leaflets of donor vesicles and acceptor vesicles attaining the

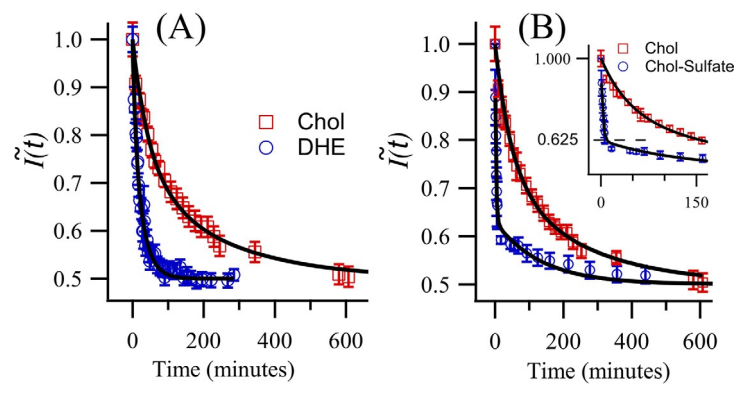


Fig. 12 (A) Comparison of normalized intensity decay curves for DHE and normal cholesterol in POPC vesicles at 50 °C. Both the flip-flop rates and exchange rates are 8–10 times faster than for cholesterol. (B) Comparison of normalized intensity decay curves for normal cholesterol and cholesterol-sulfate in POPC vesicles at 50 °C. The inset highlights the point where the outer leaflets of the donor and acceptor vesicles have the same composition, but the inner leaflets remain unchanged from their initial state, producing an intensity of 0.625. The long tail that follows is due to slow flip-flop of the sterol in the bilayer. *Figure is reproduced from Garg, S., Porcar, L., Woodka, A. C., Butler, P. D., & Perez-Salas, U.* (2011). Noninvasive neutron scattering measurements reveal slower cholesterol transport in model lipid membranes. *Biophysical Journal,* 101(2), 370–377. doi:10.1016/j.bpj.2011.06.014.

same sterol composition but where the inner leaflets' composition has not changed; i.e., the inner leaflet of donor and acceptor vesicles is the same as it was at t=0, and therefore 75% of the sterol is still in the donor vesicles while 25% (residing in the outer leaflet) has moved to the acceptor vesicles. The normalized intensity change from 0.625 to 0.5 is slow, indicative of the slow flip-flop process. Interestingly, we found that the flip-flop rate for cholesterol sulfate was similar to that of cholesterol (Garg et al., 2011).

Sterols are critical for diverse functions in cells: structurally, for signaling as well as biochemically, as these are precursors of, for example, hormones and steroids (Ikonen & Jansen, 2008; Menon, 2018). From the results presented above, we find that the transport properties of sterols can be significantly different. Therefore, how the cell transports and distributes these sterols is possibly not via a "one-size fits all" mechanism. For example, DHE and cholesterol sulfate transfer between membranes very fast while cholesterol is slow, so their transfer mechanisms are surely different. In terms of their distribution across membranes, they may be facilitated by the sterol's structure, like in the case cholesterol sulfate, but other mechanisms—still unknown—are surely provided by other characteristics

of the membrane, as is likely the case for DHE. A detail study of sterol structure characteristics and how these impact transport behavior could help elucidate sterol traffic pathways.

MD simulations studying the effects of different chemical modifications on sterols have found also great variability in both flip-flop rates (Atkovska et al., 2018; Dickey & Faller, 2007; Parisio, Sperotto, & Ferrarini, 2012) and their desorption rate from the membrane (Atkovska et al., 2018). The work of Atkovska et al., who studied 26 steroids, highlights a kinetics spectrum that is broad and that varies by orders of magnitude (Atkovska et al., 2018). To compare to the data presented here, they find that changing the hydroxyl group for a sulfate group in the steroid pregnenolone produces it to desorb fast from the membrane, a difference of 8-9 orders of magnitude compared to cholesterol, while the flip-flop rate remains similar to cholesterol (in their study, cholesterol flip-flop is fast). These trends are qualitatively similar to our measurements of cholesterol sulfate and cholesterol. In the case of DHE, their study shows that both the desorption rate from the membrane and the flip-flop rate increase by a factor \sim 10 compared to cholesterol. Interesitingly, even if the rates do not agree with our measurements, we also obtained that DHE flips and exchanges \sim 10 faster than cholesterol. Hence, it is expected that the rational for the kinetics they observe, which follow cyclohexane/water and membrane/ water partition coefficients—except for long-tailed steroids, which have an increased membrane affinity and therefore a greatly decreased membrane exiting rate—will hold in concomitant, yet to be reported, experiments.

4.3 Decoupling exchange from flip-flop

From TR-SANS measurements, we have shown that it is possible to obtain transport characteristics of the exchange of lipids and sterols between membranes in situ, and, if rate limiting, the flip-flop between leaflets without the need of perturbative tags. Even though the experimental results are robust, shown to have statistical confidence (using tools like the Akaike information criterion (Burnham & Anderson, 2002)), the results do occur while two processes, of possibly similar time scales, are happening simultaneously. Further, despite the evidence that the transport kinetic model based on exchange and flipping from donor-to-acceptor vesicles agrees extremely well with the experimental data, we have not yet unambiguously demonstrated an asymmetric composition in the bilayer while the exchange is occuring. Hence analysis of the compositional changes over time relies

more on mathematical fitting having statistical significance than in our ability to distinguish these two processes "by eye." Indeed, in cases where the two kinetic processes are naturally separated by an order of magnitude, flipping being slow and exchange being fast, the two are clearly visually separated, as are the case shown in Figs. 7 and 12B, and consequently prone to agree with our hypothesis. If not, decoupling the two processes becomes an important goal in these types of measurements to confirm the numbers obtained.

4.3.1 Studying lipid flip-flop in asymmetric vesicles

Studying composition asymmetry across the lipid bilayer has been an important goal to understand the consequences of two lipid leaflets having different physicochemical properties. Examples are, the mechanisms of interleaflet coupling in the context of overall mechanical properties and well as in the formation of lipid domains (London, 2019; Weiner & Feigenson, 2019) or in membrane dynamics, such as bending fluctuations, in particular as they compare to those of symmetric membranes (Blumer et al., 2020; Rickeard et al., 2020). Several approaches have been developed to create asymmetric membranes to be studied by optical, spectroscopic and scattering techniques and some of these strategies have been recently reviewed by Scott et al. (Scott et al., 2021). Neutron scattering stands out as a particularly well suited technique to studying leaflet compositional asymmetry and its changes through flip-flop, in situ.

SANS/TR-SANS is sensitive at discerning lipid composition differences across the lipid bilayer because the scattering signal from vesicles allows for the retrieval of structure information of individual leaflets in the high Q region of the spectra as shown in Fig. 1B. In order to extract this information, contrast between leaflets, reflecting their compositional asymmetry, is key and this is provided by the use of hydrogenated and deuterated lipids. The high Q of the scattering plot shown in Fig. 13 displays a highly asymmetric dDPPC/hDPPC distribution across the leaflets of the vesicles with the characteristic up-lift in the scattering. In this case, the outer leaflet is enriched with hDPPC while the inner leaflet is enriched with dDPPC as obtained from the fit and shown in the SLD profile plot. Indeed, upon allowing the flip-flop process to proceed, the membrane becomes symmetric in composition and the intensity in this Q region also drops producing the typical signature of symmetric vesicles. Hence SANS can unambiguously determine the lipid composition in each leaflet as shown in Fig. 13.

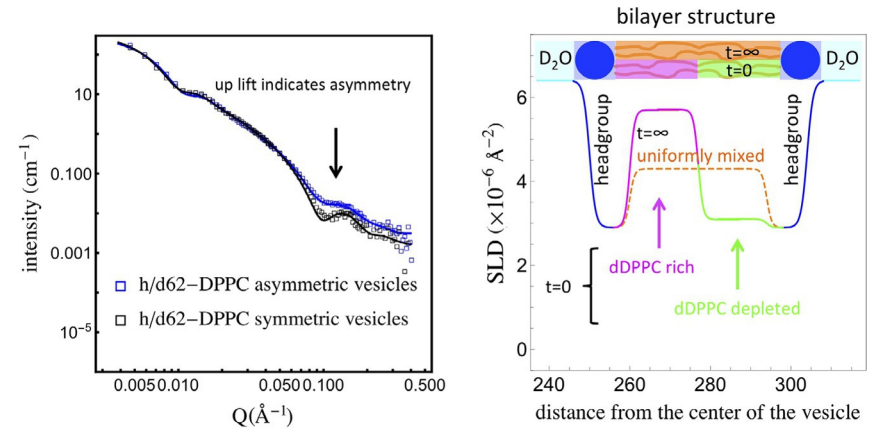


Fig. 13 Left, SANS scattering curves with tight collimation to resolve bilayer features. The vesicles are in D_2O to have the lowest possible background. The scattering from asymmetric vesicles have the characteristic up-lift in the scattering (blue). Upon mixing, due to lipid flip flop, the scattering develops a well-defined minimum characteristic of a symmetric bilayer (black). The lines through the data correspond to fits showing the change in the composition in each leaflet between the initial and final bilayer configurations, as shown on the SLD profile on the right. Figure on the left is reproduced from Liu, Y., Kelley, E. G., Batchu, K. C., Porcar, L., & Perez-Salas, U. (2020). Creating asymmetric phospholipid vesicles via exchange with lipid-coated silica nanoparticles. Langmuir, 36(30), 8865–8873. doi:10.1021/acs.langmuir.0c01188.

While the scattering analysis and the corresponding asymmetric composition can be resolved by SANS straightforwardly, the experimental methods to produce asymmetric bilayers are not as straight forward. Several approaches have emerged as pathways to creating a single monodisperse population of unilamellar vesicles having the same asymmetric lipid distribution. One technique that has proven to be robust for SANS/ TR-SANS measurements consists of utilizing cyclodextrin (CD) molecules. CDs directly interact with membranes. These compounds are used to deplete or add lipids and sterols to model (StClair, Wang, Li, & London, 2017) and cell membranes (Zidovetzki & Levitan, 2007). CDs are used in the treatment of lipid diseases (Coisne et al., 2016) like Niemann pick disease type C (Matencio, Navarro-Orcajada, Gonzalez-Ramon, Garcia-Carmona, & Lopez-Nicolas, 2020), as well as cancer (Qiu, Li, & Liu, 2017) and SARS-COV-2 (Fatmi, Taouzinet, Skiba, & Iguer-Ouada, 2021). CDs, in fact, have a broad applicability (Fourmentin, 2018) because they are small molecules that are soluble in an aqueous environment but can host hydrophobic molecules in their inner barrel-like core (Scott et al., 2021).

For the purpose of creating asymmetric unilamellar vesicles, the method consists of using a donor lipid population that exchanges lipids with an acceptor vesicle population where the exchange happens through the CD carriers. CDs only change the composition of the outer leaflet of the acceptor vesicles by enriching it with donor lipids (Doktorova et al., 2018; Markones et al., 2018; Scott et al., 2021). It has also been shown that the method can be applied to generate asymmetric vesicles with peptides (Nguyen, DiPasquale, Rickeard, Doktorova, et al., 2019) and fully functional integrated proteins (Markones et al., 2020) pre-embedded in the vesicles.

Notwithstanding, we found that in the case of cholesterol, as shown in Fig. 14, the presence of CD not only produced a highly accelerated exchange rate between donor and acceptor vesicles, it also produced a highly accelerated flip-flop rate. As a result, we devised a completely different strategy to producing asymmetric membranes, one in which we take advantage of the fact that lipids do diffuse freely through an aqueous environment and follow well-defined thermodynamic properties. The strategy consists of combining lipid coated nanoparticles (we used silica nanoparticles) and vesicles at a ratio dominated by the donor population (lipid coated nanoparticles). By using a very unequal ratio of donors to acceptors, as described by Eqs. (13a) and (13c), it is possible to build high compositional asymmetry in the acceptor vesicle population while not affecting the flip-flop process. The lipid-coated nanoparticles, having a higher density

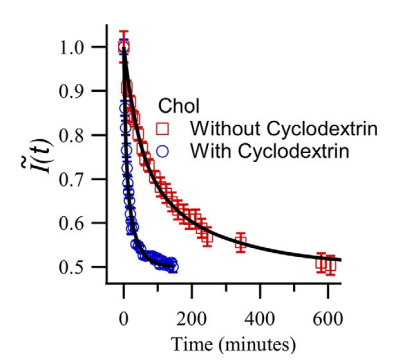


Fig. 14 Comparison of normalized intensity decay curves for cholesterol in POPC vesicles with and without the presence of 2 mM cyclodextrin (CD) at 50 °C. *Figure is reproduced from Garg, S., Porcar, L., Woodka, A. C., Butler, P. D., & Perez-Salas, U.* (2011). Noninvasive neutron scattering measurements reveal slower cholesterol transport in model lipid membranes. *Biophysical Journal, 101(2), 370–377. doi:10.1016/j. bpj.2011.06.014.*

than the vesicles, are removed by centrifugation, leaving behind the asymmetric vesicle population. Our proof-of-principle measurements are shown in Fig. 13 (Liu et al., 2020). In this study, which was complemented with ¹H NMR measurements (which is also sensitive to isotopic labeling and can probe the distribution of hydrogenated and deuterated molecules in a lipid bilayer (Marquardt et al., 2017)), we found that the rate of flip-flop of DPPC, was consistent to the flip-flop rates found in asymmetric vesicles that used the CD approach (Liu et al., 2020). Hence, at least for DPPC and other long chain phospholipids, CDs may not produce additional or significant interleaflet scrambling at low CD concentration (Nakano et al., 2009). However, the case shown in Fig. 14 for cholesterol highlights awareness of possible biases induced by CDs (Zidovetzki & Levitan, 2007) and the need to have alternative approaches.

4.3.2 Studying lipid exchange and flip-flop in single membranes

Techniques that can directly probe the structure of a single lipid bilayer deposited on a surface like neutron reflectometry (NR) or sum frequency generation vibrational spectroscopy (SFGVS) were seen as ideal to follow flip-flop and exchange on a single membrane. In addition, both techniques are sensitive to isotopic labeling and can probe the replacement and displacement of protiated and deuterated molecules in the membrane. With high spatial resolution (<1 nm) and a temporal resolution of minutes, with SFGVS and NR it is possible to follow the spontaneous loss of asymmetry via lipid flip-flop in asymmetric bilayers (Allhusen & Conboy, 2017; Gerelli, Porcar, & Fragneto, 2012). With NR it is also possible to monitor the presence of asymmetric intermediates during experiments involving lipid exchange between vesicles in solution and a single bilayer on a surface (Gerelli et al., 2013).

Using this latter approach, we deposited a symmetric SLB on a solid substrate (usually a large ($\sim 40\,\mathrm{cm}^2$) and highly polished (rms roughness $\sim 0.3\,\mathrm{nm}$) silicon crystals with a thin (1 nm) silicon oxide layer) via vesicle fusion which was then exposed to a solution of vesicles composed by the same phospholipid but having the complementary deuteration form. This type of experiment was developed to mimic the measurement of the transfer of lipids between membranes (in vesicles) with TR-SANS with the additional advantage of directly monitoring composition changes in a single membrane. In the case of DMPC, reported to flip slow in DMPC membranes using TR-SANS by Nakano et al. (Nakano et al., 2007), we found

that flip-flop was inaccessible. However, we were able to recapitulate the results obtained by Nakano et al. for lipid exchange, including the energetics.

Asymmetric SLB can also be formed, one leaflet at a time, on a solid substrate by Langmuir-Blodgett and Langmuir-Schaefer deposition techniques. Using this approach, we studied asymmetric SLB that either had the same phospholipids (DPPC/dDPPC) or different ones (DMPC/dDSPC). These layers were deposited in the gel phase where they remained asymmetric until lipid flip-flop was activated by increasing the sample's temperature, i.e., by crossing the gel-to-fluid phase transition temperature of the system. The phase transition from gel to the fluid phase behavior, which is normally sharp in vesicles, it is broad in SLBs (Gerelli, 2019), and this influences the activation and progression of lipid flip-flop, which adds complexity to the experimental analysis (Porcar & Gerelli, 2020).

Unfortunately, for both approaches, the "surface" was found to accelerate lipid flipping (Gerelli et al., 2012; Porcar & Gerelli, 2020). While in defect-free supported membranes on silica nanoparticles we find that fast flip-flop is driven by the surface's induced disorder of chain packing (Wah et al., 2017), as evidenced from the surface induced broad melting temperature behavior on flat surfaces (Gerelli, 2019) and as needed in NR experiments (or sum vibrational spectroscopy), SLB have additional unavoidable membrane defects—membrane discontinuities (Marquardt et al., 2017)—that accelerate flipping by several orders of magnitude and producing a lower activation energy (Porcar & Gerelli, 2020). Notwithstanding, in lipids that flip-flop very slowly, like DPPC, it is still possible to capture membrane asymmetry as shown in Fig. 15, and therefore the technique could still provide a platform to study asymmetry in membranes (Porcar & Gerelli, 2020).

4.4 Lipid exchange and flip-flop behavior in the presence of biological agents

Although cells use proteins and other molecular transporters to regulate the distribution of lipids across membranes (Kobayashi & Menon, 2018), membranes are also targets of biological agents which may alter this distribution (Doktorova et al., 2020; Lohner, 2017). An example of important/critical biological agents that interact with membranes are antimicrobial peptides (AMPs). Antimicrobial peptides are, as its name suggests, small molecules, ubiquitous in nature, that are an important part in the immune system of different organisms and which have inhibitory effects against bacteria, fungi,

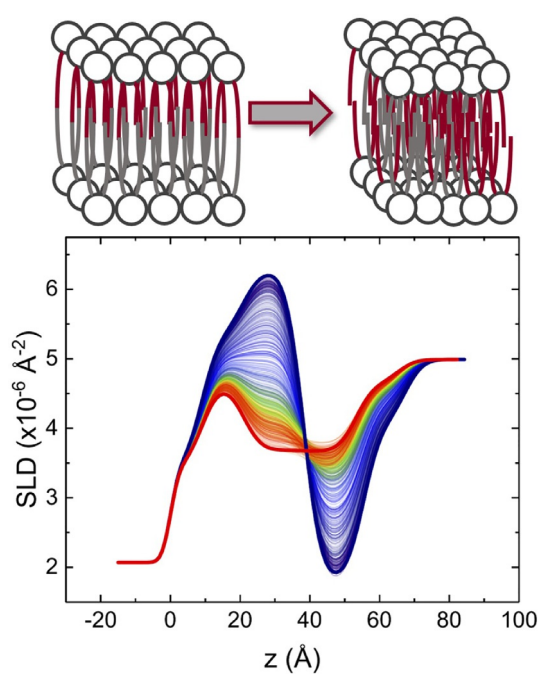


Fig. 15 Top: Schematic representation of initial asymmetric SLB in gel phase and final fully symmetric SLB in fluid phase. Different colors indicate deuterated and protiated phospholipid molecules. Bottom: Collection of scattering length density profiles along the normal direction to the bilayer surface ($z \approx 40 \, \text{Å}$ indicate the SLB mid-plane). The initial asymmetric structure is represented with the blue thick line while the final symmetric system is represented by the thick red line. Intermediate curves collected at different times and temperatures clearly indicate the gradual loss of symmetry. Readapted from Porcar, L., & Gerelli, Y. (2020). On the lipid flip-flop and phase transition coupling. Soft Matter, 16(33), 7696–7703. doi:10.1039/d0sm01161d.

parasites and viruses. In addition, the advent of antibiotic-resistant microorganisms and the increasing concern in the use of antibiotics, has resulted in the development of de novo AMPs (Vishnepolsky et al., 2019) which have potential protective use in humans, animals and plants (Huan, Kong, Mou, & Yi, 2020). Thus, there is great impetuous to understand their mechanisms of action especially because these do not follow a direct lock-and-key mechanism that makes antibiotics susceptible to the development of resistance (Wimley & Hristova, 2011). As recently shown by Marx et al. (Marx, Frewein, et al., 2021; Marx, Semeraro, et al., 2021), connecting peptide activity in bacteria with its activity on model membrane mimics is intricate. Notwithstanding, as the authors emphasize, membrane characteristics do play an important role in the translocation of the peptide into cells,

and hence studies in understanding peptide-lipid-membrane structure interactions are important. TR-SANS studies that have examined how these molecules affect the movement of lipids between and within membranes have found that, independent of AMP structure, their presence accelerates lipid flip-flop (Marx, Frewein, et al., 2021; Marx, Semeraro, et al., 2021; Nguyen, DiPasquale, Rickeard, Doktorova, et al., 2019) as well as the exchange of lipids between membranes (Nakao et al., 2021; Nguyen et al., 2021; Nielsen et al., 2021, 2020). In these studies, the authors looked at pre-inserted peptides as well as free peptides that interact with membranes—which being cationic, interact electrostatically with membranes—and found that in the latter case the effect is near instantaneous, while in the former it proceeds much slower, but faster than when no peptides are present (Nguyen, DiPasquale, Rickeard, Doktorova, et al., 2019). The combined results from the work of these groups of researchers shows that these molecules share certain features that allow them to disrupt membranes by promoting the transport of lipids between and within membranes despite differences in structure and in how they interact with membranes.

As it is always the case, possible sources of bias have to be identified and parsed out from peptide action, such as the—separate—effect of co-solvents commonly used in these studies (Nguyen, DiPasquale, Rickeard, Doktorova, et al., 2019). Indeed solvents, such as short-chain alkanes, are known to modify membrane properties in vitro (Ly & Longo, 2004) and in vivo (Goldstein, 1986) as well as accelerate lipid exchange and flip-flop, as recently reported by Nguyen et al. for methanol (Nguyen, DiPasquale, Rickeard, Stanley, et al., 2019). Indeed solvents having low solubility in water with preferential partitioning into membranes, enhance these effects (Dickey & Faller, 2007). Fig. 16 shows the dramatic increase in the transport characteristics of hDMPC between CM dDMPC membranes in the presence of butanol, a low solubility solvent in water.

Another example of physiological interest is the interaction of plasma lipoprotein particles—low and high-density lipoprotein particles (LDL and HDL)—with plasma membranes. HDL and LDL are currently used as clinical markers for atherosclerosis, a disease in which plaques of lipids and fibrous elements accumulate in the blood vessels (Carmena, Duriez, & Fruchart, 2004; Lusis, 2000). Therefore, the mechanism of lipid exchange between HDL and LDL particles with cellular membranes needs to be carefully examined at a molecular level in order to understand how they

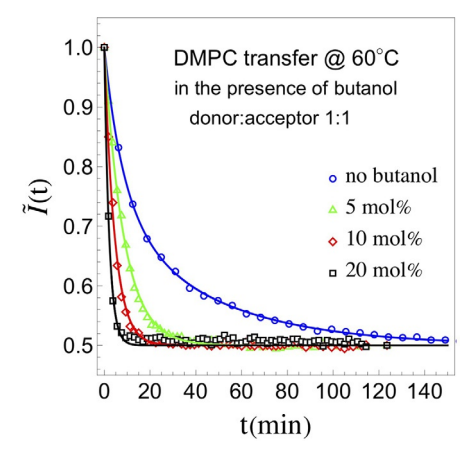


Fig. 16 Normalized total intensity decay curves for hDMPC in CM dDMPC vesicles with and without butanol. Butanol's molar concentration represents the total number of Butanol molecules/(total number of DMPC molecules+Alcohol molecules). DMPC concentration in the solution was 40 mg/mL.

participate in the buildup of arterial plaques. A study by Maric et al., using TR-SANS, followed the lipid exchange between human HDL and LDL particles and cellular membrane mimics (vesicles), which, through deuteration and contrast matching, were "invisible" to neutrons (Maric et al., 2019). The data they obtained shows that, in addition to lipid exchange through monomer diffusion, the exchange also occurs through collisions and tethering, which also depends on the apolipoprotein type. They find that the exchange of lipids between cell membrane mimics and HDL particles is more efficient than with LDL particles. The authors associate tethering efficiency to their envelope protein density. Indeed, HDL have a larger concentration of envelope ApoA proteins while LDL particles have a lower ApoB protein content.

Lipid transport is also an important consideration when using lipid-based scaffolds for membrane protein studies. Lipid nanodiscs consist of a protein or a polymer or a detergent "belt" surrounding a nanometer (\sim 3 to \sim 30 nm) lipid bilayer patch. Lipid nanodiscs have become the method of choice as a stabilizing scaffold for membrane proteins used in protein structural studies (Denisov & Sligar, 2017). In addition, lipid nanodiscs are used in many other applications, such as high-throughput screening and diagnostics or carriers of hydrophobic therapeutics, to mention some (Ryan, 2010). Differences exist between nanodiscs, particularly as it relates to the belt and its interaction with lipids. Specific lipid associations with the transmembrane domain of

membrane proteins, like those commonly found with phosphatidylinositol, may be altered by the belt. TR-SANS has thus been used to assess the ease of movement of lipids between nanodics to understand lipid stability. Overall, it is found that between nanodiscs lipids move faster than between vesicles (Nakano, Fukuda, Kudo, Miyazaki, et al., 2009; Xia et al., 2015). Further, different belt strategies for the nanodiscs can also produce large differences in the exchange kinetics of lipids, as recently highlighted by Cuevas et al. (Cuevas Arenas et al., 2017). They find that polymer-based belt nanodiscs produce the most disorder of the lipid bilayer and therefore the fastest exchange of lipids between nanodiscs, which, they suggest, could be used advantageously to be able to only keep those lipids that strongly associate with the protein while excluding those with weaker contacts.

5. Current and future perspectives

Eukaryotic cells generate thousands of chemically distinct lipids (Sud et al., 2007) from which the membranes of organelles, including the PM, can be built. These lipids confer these membranes with not only different physical properties but also host distinct functions. Interestingly, the mapping of the distribution of lipids across organelle membranes reflects the secretory pathway established by evolution (van Meer, 1989; Voelker, 1991). Key in preserving the homeostatic balance of cell membranes is the machinery that distributes lipids—with high sensitivity—from their place of synthesis, mostly in the endoplasmic reticulum, to their target membrane and eventual disposal (Blom, Somerharju, & Ikonen, 2011; Holthuis & Menon, 2014; Lev, 2010; Voelker, 1990). This machinery, however, is constantly battling equilibrium, where entropy of mixing drives homogenization (Callan-Jones, Sorre, & Bassereau, 2011). Lipid architecture, lipid-lipid and lipid-protein interactions, as we are finding out, have built-in passive regulatory roles in maintaining a relatively stable membrane organization over hours or days, therefore aiding in the cost of its maintenance. It has been recognized for many decades that understanding these interactions including how they change—rapidly—as a result of signaling (Doktorova et al., 2020) or fail with the onset of disease (Goldberg & Riordan, 1986; Maxfield & Tabas, 2005) will provide a molecular-based tool to detect and possibly address health in the membrane.

TR-SANS clearly stands out as a powerful technique to follow the movement of lipids between and within membranes and extract the

time-scales and energetics for maintaining compositionally distinct membranes. This is critical information to map out the built-in mechanisms of passive regulation of membranes. In addition, it can also detect and follow in situ how these gradients are affected by the presence of peptides, proteins or other molecules. The work in this regard is new because of breakthroughs in identifying and resolving experimental biases, on the one hand, but also in producing systems that had not been accessible before, like asymmetric vesicles. Deuteration capabilities will expand the complexity of the systems studied, which together with advances in protein expression and purification of membrane proteins, will open the road for detailed work on the lipid transport machinery itself, such as the action of flippases and scamblases, which is ultimately directly responsible of maintaining the homeostatic state of cell membranes.

As already alluded to, scattering techniques have to be pursued in combination with other techniques (e.g., NMR, calorimetry, gas chromatography to name a few (Liu et al., 2020)) that provide additional information for data analysis or checks. Most importantly, as recently shown by Marx et al. (Marx, Frewein, et al., 2021; Marx, Semeraro, et al., 2021), the goal is to seek congruency between experiments at different scales (molecular models to cells). It is certainly now common or even expected that molecular biology studies be combined with a powerful theoretical tool like MD simulations and scattering studies of membranes are no exception (Ashkar et al., 2018; Gupta & Ashkar, 2021). In hand with experiements, advances in MD simulations are allowing current efforts to simulate physiologically relevant membranes (Khakbaz & Klauda, 2015; Marrink et al., 2019).

The scattering techniques described herein are provided by large-scale government sponsored facilities, and appear hard to access, but they are not. Access is free once a peer-reviewed proposal has been allotted beamtime. The scientific staff will help new users build scattering expertize in support of their research program. Admittedly, the largest barrier to using scattering more broadly is the need of extensive data modeling. There is a significant effort to utilize complex algorithms (Treece et al., 2019) to streamline the analysis and to conceivably incorporate multiple data sets from different experimental techniques. This work is being provided by the scattering community at large as well as directly from scientific staff at facilities to make the technique accessible to none experts (Doucet et al., 2021; Lewis-Laurent, Doktorova, Heberle, & Marquardt, 2021). Hence, the future is bright for scattering techniques as they become utilized to their full potential to understand cell membranes and beyond.

Acknowledgments

This work utilized the facilities at the National Institute for Standards and Technology, supported in part by the National Science Foundation under agreement no. DMR-0454672. Commercial materials or equipment if identified in this paper do not imply recommendation or endorsement by the National Institute of Standards and Technology nor should be identified as the best available for the purpose. The authors thank the Institute Laue Langevin for providing neutron beam time under DOI:10.5291/ILL-DATA.9-13-823. U.P.-S. additionally acknowledges travel support from the ILL to promote scientific collaboration with L. Porcar, Y. Gerelli, and G. Fragneto. U.P.-S. gratefully acknowledges the support from the NSF CAREER award DMR-1753238.

References

- Allhusen, J. S., & Conboy, J. C. (2017). The ins and outs of lipid Flip-flop. *Accounts of Chemical Research*, 50(1), 58–65. https://doi.org/10.1021/acs.accounts.6b00435.
- Anglin, T. C., & Conboy, J. C. (2009). Kinetics and thermodynamics of flip-flop in binary phospholipid membranes measured by sum-frequency vibrational spectroscopy. *Biochemistry*, 48(43), 10220–10234. https://doi.org/10.1021/bi901096j.
- Ano, Y., & Nakayama, H. (2018). Preventive effects of dairy products on dementia and the underlying mechanisms. *International Journal of Molecular Sciences*, 19(7). https://doi.org/ 10.3390/ijms19071927.
- Ashkar, R., Bilheux, H. Z., Bordallo, H., Briber, R., Callaway, D. J. E., Cheng, X., et al. (2018). Neutron scattering in the biological sciences: Progress and prospects. Acta Crystallographica Section D: Structural Biology, 74(Pt 12), 1129–1168. https://doi.org/10. 1107/S2059798318017503.
- Atkovska, K., Klingler, J., Oberwinkler, J., Keller, S., & Hub, J. S. (2018). Rationalizing steroid interactions with lipid membranes: Conformations, partitioning, and kinetics. ACS Central Science, 4(9), 1155–1165. https://doi.org/10.1021/acscentsci.8b00332.
- Backer, J. M., & Dawidowicz, E. A. (1981). Transmembrane movement of cholesterol in small unilamellar vesicles detected by cholesterol oxidase. *The Journal of Biological Chemistry*, 256(2), 586–588 (Retrieved from http://www.ncbi.nlm.nih.gov/pubmed/6935193).
- Baral, S., Levental, I., & Lyman, E. (2020). Composition dependence of cholesterol flip-flop rates in physiological mixtures. *Chemistry and Physics of Lipids*, 232, 104967. https://doi. org/10.1016/j.chemphyslip.2020.104967.
- Bennett, W. F., MacCallum, J. L., Hinner, M. J., Marrink, S. J., & Tieleman, D. P. (2009). Molecular view of cholesterol flip-flop and chemical potential in different membrane environments. *Journal of the American Chemical Society*, 131(35), 12714–12720. https://doi.org/10.1021/ja903529f.
- Bennett, W. F., MacCallum, J. L., & Tieleman, D. P. (2009). Thermodynamic analysis of the effect of cholesterol on dipalmitoylphosphatidylcholine lipid membranes. *Journal of the American Chemical Society*, 131(5), 1972–1978. https://doi.org/10.1021/ja808541r.
- Bennett, W. F., & Tieleman, D. P. (2012). Molecular simulation of rapid translocation of cholesterol, diacylglycerol, and ceramide in model raft and nonraft membranes. *Journal of Lipid Research*, 53(3), 421–429. https://doi.org/10.1194/jlr.M022491.
- Blom, T., Somerharju, P., & Ikonen, E. (2011). Synthesis and biosynthetic trafficking of membrane lipids. *Cold Spring Harbor Perspectives in Biology*, *3*(8), a004713. https://doi.org/10.1101/cshperspect.a004713.

- Blumer, M., Harris, S., Li, M., Martinez, L., Untereiner, M., Saeta, P. N., et al. (2020). Simulations of asymmetric membranes illustrate cooperative leaflet coupling and lipid adaptability. *Frontiers in Cell and Development Biology*, 8, 575. https://doi.org/10.3389/fcell.2020.00575.
- Brasaemle, D. L., Robertson, A. D., & Attie, A. D. (1988). Transbilayer movement of cholesterol in the human-erythrocyte membrane. *Journal of Lipid Research*, 29(4), 481–489.
- Breidigan, J. M., Krzyzanowski, N., Liu, Y., Porcar, L., & Perez-Salas, U. (2017). Influence of the membrane environment on cholesterol transfer. *Journal of Lipid Research*, 58(12), 2255–2263. https://doi.org/10.1194/jlr.M077909.
- Bretscher, M. S. (1972). Asymmetrical lipid bilayer structure for biological membranes. *Nature: New Biology*, 236(61), 11–12 (Retrieved from http://www.ncbi.nlm.nih.gov/pubmed/4502419).
- Bruckner, R. J., Mansy, S. S., Ricardo, A., Mahadevan, L., & Szostak, J. W. (2009). Flip-flop-induced relaxation of bending energy: Implications for membrane remodeling. *Biophysical Journal*, 97(12), 3113–3122. https://doi.org/10.1016/j.bpj.2009.09.025.
- Bryant, G., Taylor, M. B., Darwish, T. A., Krause-Heuer, A. M., Kent, B., & Garvey, C. J. (2019). Effect of deuteration on the phase behaviour and structure of lamellar phases of phosphatidylcholines deuterated lipids as proxies for the physical properties of native bilayers. *Colloids and Surfaces. B, Biointerfaces*, 177, 196–203. https://doi.org/10.1016/j.colsurfb.2019.01.040.
- Burnham, K. P., & Anderson, D. R. (2002). Model selection and inference: A practical information-theoretic approach (2nd ed.). New York: Springer-Verlag.
- Buwaneka, P., Ralko, A., Liu, S.-L., & Cho, W. (2021). Evaluation of the available cholesterol concentration in the inner leaflet of the plasma membrane of mammalian cells. *Journal of Lipid Research*, 62, 100084. https://doi.org/10.1016/j.jlr.2021.100084.
- Callan-Jones, A., Sorre, B., & Bassereau, P. (2011). Curvature-driven lipid sorting in biomembranes. Cold Spring Harbor Perspectives in Biology, 3(2). https://doi.org/10. 1101/cshperspect.a004648.
- Carbone, C. B., Kern, N., Fernandes, R. A., Hui, E., Su, X., Garcia, K. C., et al. (2017). In vitro reconstitution of T cell receptor-mediated segregation of the CD45 phosphatase. Proceedings of the National Academy of Sciences of the United States of America, 114(44), E9338–E9345. https://doi.org/10.1073/pnas.1710358114.
- Carmena, R., Duriez, P., & Fruchart, J. C. (2004). Atherogenic lipoprotein particles in atherosclerosis. *Circulation*, 109(23 Suppl 1), III2–7. https://doi.org/10.1161/01.CIR.0000131511.50734.44.
- Chakraborty, S., Doktorova, M., Molugu, T. R., Heberle, F. A., Scott, H. L., Dzikovski, B., et al. (2020). How cholesterol stiffens unsaturated lipid membranes. *Proceedings of the National Academy of Sciences*, 117(36), 21896–21905. https://doi.org/10.1073/pnas. 2004807117.
- Choi, S. H., Bates, F. S., & Lodge, T. P. (2011). Molecular exchange in ordered Diblock copol-ymer micelles. *Macromolecules*, 44(9), 3594–3604. https://doi.org/10.1021/ma102788v.
- Choi, S. H., Lodge, T. P., & Bates, F. S. (2010). Mechanism of molecular exchange in diblock copolymer micelles: Hypersensitivity to core chain length. *Physical Review Letters*, 104(4), 047802. https://doi.org/10.1103/PhysRevLett.104.047802.
- Coisne, C., Tilloy, S., Monflier, E., Wils, D., Fenart, L., & Gosselet, F. (2016). Cyclodextrins as emerging therapeutic tools in the treatment of cholesterol-associated vascular and neurodegenerative diseases. *Molecules*, 21(12). https://doi.org/10.3390/molecules21121748.
- Courtney, K. C., Pezeshkian, W., Raghupathy, R., Zhang, C., Darbyson, A., Ipsen, J. H., et al. (2018). C24 sphingolipids govern the Transbilayer asymmetry of cholesterol and lateral organization of model and live-cell plasma membranes. *Cell Reports*, 24(4), 1037–1049. https://doi.org/10.1016/j.celrep.2018.06.104.

Cuevas Arenas, R., Danielczak, B., Martel, A., Porcar, L., Breyton, C., Ebel, C., et al. (2017). Fast collisional lipid transfer among polymer-bounded Nanodiscs. *Scientific Reports*, 7, 45875. https://doi.org/10.1038/srep45875.

- Darwish, T. A., Luks, E., Moraes, G., Yepuri, N. R., Holden, P. J., & James, M. (2013). Synthesis of deuterated [D32]oleic acid and its phospholipid derivative [D64]dioleoyl-sn-glycero-3-phosphocholine. *Journal of Labelled Compounds and Radiopharmaceuticals*, 56(9–10), 520–529. https://doi.org/10.1002/jlcr.3088.
- Dawoud, M., & Abdou, R. (2021). Ion exchange column technique as a novel method for evaluating the release of docetaxel from different lipid nanoparticles. *Drug Delivery and Translational Research*. https://doi.org/10.1007/s13346-021-00937-2.
- Denisov, I. G., & Sligar, S. G. (2017). Nanodiscs in membrane biochemistry and biophysics. *Chemical Reviews*, 117(6), 4669–4713. https://doi.org/10.1021/acs.chemrev.6b00690.
- Devaux, P. F., & Morris, R. (2004). Transmembrane asymmetry and lateral domains in biological membranes. *Traffic*, 5(4), 241–246. https://doi.org/10.1111/j.1600-0854.2004. 0170.x.
- Dickey, A. N., & Faller, R. (2007). How alcohol chain-length and concentration modulate hydrogen bond formation in a lipid bilayer. *Biophysical Journal*, *92*(7), 2366–2376. https://doi.org/10.1529/biophysj.106.097022.
- Doktorova, M., Heberle, F. A., Eicher, B., Standaert, R. F., Katsaras, J., London, E., et al. (2018). Preparation of asymmetric phospholipid vesicles for use as cell membrane models. *Nature Protocols*, 13(9), 2086–2101. https://doi.org/10.1038/s41596-018-0033-6.
- Doktorova, M., Symons, J. L., & Levental, I. (2020). Structural and functional consequences of reversible lipid asymmetry in living membranes. *Nature Chemical Biology*, 16(12), 1321–1330. https://doi.org/10.1038/s41589-020-00688-0.
- Doucet, M., Cho, J. H., Alina, G., Attala, Z., Bakker, J., Bouwman, W., et al. (2021). SASview. Zenodo.
- Efimova, Y. M., Haemers, S., Wierczinski, B., Norde, W., & van Well, A. A. (2007). Stability of globular proteins in H2O and D2O. *Biopolymers*, 85(3), 264–273. https://doi.org/10.1002/bip.20645.
- Eicher, B., Heberle, F. A., Marquardt, D., Rechberger, G. N., Katsaras, J., & Pabst, G. (2017). Joint small-angle X-ray and neutron scattering data analysis of asymmetric lipid vesicles. *Journal of Applied Crystallography*, 50(Pt 2), 419–429. https://doi.org/10.1107/S1600576717000656.
- Eyring, H. (1935). The activated complex in chemical reactions. *Journal of Chemical Physics*, 3(2). https://doi.org/10.1063/1.1749604.
- Fadok, V. A., Voelker, D. R., Campbell, P. A., Cohen, J. J., Bratton, D. L., & Henson, P. M. (1992). Exposure of phosphatidylserine on the surface of apoptotic lymphocytes triggers specific recognition and removal by macrophages. *Journal of Immunology*, 148(7), 2207–2216 (Retrieved from https://www.ncbi.nlm.nih.gov/pubmed/1545126).
- Fatmi, S., Taouzinet, L., Skiba, M., & Iguer-Ouada, M. (2021). The use of Cyclodextrin or its complexes as a potential treatment against the 2019 novel coronavirus: A mini-review. Current Drug Delivery, 18(4), 382–386. https://doi.org/10.2174/ 1567201817666200917124241.
- Fourmentin, S. (2018). Cyclodextrin applications in medicine, food, environment and liquid crystals. New York, NY: Springer Berlin Heidelberg.
- Garg, S., Castro-Roman, F., Porcar, L., Butler, P., Bautista, P. J., Krzyzanowski, N., et al. (2014). Cholesterol solubility limit in lipid membranes probed by small angle neutron scattering and MD simulations. *Soft Matter*, 10(46), 9313–9317. https://doi.org/10. 1039/c4sm01219d.

- Garg, S., Porcar, L., Woodka, A. C., Butler, P. D., & Perez-Salas, U. (2011). Noninvasive neutron scattering measurements reveal slower cholesterol transport in model lipid membranes. *Biophysical Journal*, 101(2), 370–377. https://doi.org/10.1016/j.bpj.2011. 06.014.
- Garg, S., Porcar, L., Woodka, A. C., Butler, P. D., & Perez-Salas, U. (2012). Response to "how slow is the Transbilayer diffusion (Flip-flop) of cholesterol?". *Biophysical Journal*, 102(4), 947–949.
- Gerelli, Y. (2019). Phase transitions in a single supported phospholipid bilayer: Real-time determination by neutron reflectometry. *Physical Review Letters*, 122(24), 248101. https://doi.org/10.1103/PhysRevLett.122.248101.
- Gerelli, Y., Porcar, L., & Fragneto, G. (2012). Lipid rearrangement in DSPC/DMPC bilayers: A neutron reflectometry study. *Langmuir*, 28(45), 15922–15928. https://doi.org/10.1021/la303662e.
- Gerelli, Y., Porcar, L., Lombardi, L., & Fragneto, G. (2013). Lipid exchange and Flip-flop in solid supported bilayers. *Langmuir*, 29(41), 12762–12769. https://doi.org/10.1021/ La402708u.
- Goldberg, D. M., & Riordan, J. R. (1986). Role of membranes in disease. Clinical Physiology and Biochemistry, 4(5), 305–336 (Retrieved from https://www.ncbi.nlm.nih.gov/ pubmed/3022980).
- Goldstein, D. B. (1986). Effect of alcohol on cellular membranes. *Annals of Emergency Medicine*, 15(9), 1013–1018. https://doi.org/10.1016/s0196-0644(86)80120-2.
- Gu, R. X., Baoukina, S., & Tieleman, D. P. (2019). Cholesterol Flip-flop in heterogeneous membranes. *Journal of Chemical Theory and Computation*, 15(3), 2064–2070. https://doi. org/10.1021/acs.jctc.8b00933.
- Gupta, S., & Ashkar, R. (2021). The dynamic face of lipid membranes. *Soft Matter*, 17(29), 6910–6928. https://doi.org/10.1039/d1sm00646k.
- Gupta, A., Korte, T., Herrmann, A., & Wohland, T. (2020). Plasma membrane asymmetry of lipid organization: Fluorescence lifetime microscopy and correlation spectroscopy analysis. *Journal of Lipid Research*, 61(2), 252–266. https://doi.org/10.1194/jlr. D119000364.
- Hamilton, J. A. (2003). Fast flip-flop of cholesterol and fatty acids in membranes: Implications for membrane transport proteins. *Current Opinion in Lipidology*, 14(3), 263–271. https://doi.org/10.1097/01.mol.0000073507.41685.9b.
- Hamley, I. W. (2021). Small-angle scattering: Theory, instrumentation, data and applications (1st ed.). Hoboken, NJ: Wiley.
- Heberle, F. A., Marquardt, D., Doktorova, M., Geier, B., Standaert, R. F., Heftberger, P., et al. (2016). Subnanometer structure of an asymmetric model membrane: Interleaflet coupling influences domain properties. *Langmuir*, 32(20), 5195–5200. https://doi.org/10.1021/acs.langmuir.5b04562.
- Heberle, F. A., & Pabst, G. (2017). Complex biomembrane mimetics on the subnanometer scale. *Biophysical Reviews*, 9(4), 353–373. https://doi.org/10.1007/s12551-017-0275-5.
- Heberle, F. A., Petruzielo, R. S., Pan, J., Drazba, P., Kucerka, N., Standaert, R. F., et al. (2013). Bilayer thickness mismatch controls domain size in model membranes. *Journal of the American Chemical Society*, 135(18), 6853–6859. https://doi.org/10.1021/ja3113615.
- Heinrich, F., Kienzle, P. A., Hoogerheide, D. P., & Losche, M. (2020). Information gain from isotopic contrast variation in neutron reflectometry on protein-membrane complex structures. *Journal of Applied Crystallography*, 53(Pt 3), 800–810. https://doi.org/10.1107/ S1600576720005634.

Holthuis, J. C., & Levine, T. P. (2005). Lipid traffic: Floppy drives and a superhighway. Nature Reviews. Molecular Cell Biology, 6(3), 209–220. https://doi.org/10.1038/nrm1591.

- Holthuis, J. C., & Menon, A. K. (2014). Lipid landscapes and pipelines in membrane homeostasis. *Nature*, 510(7503), 48–57. https://doi.org/10.1038/nature13474.
- Homan, R., & Pownall, H. J. (1988). Transbilayer diffusion of phospholipids: Dependence on headgroup structure and acyl chain length. *Biochimica et Biophysica Acta*, *938*(2), 155–166 (Retrieved from http://www.ncbi.nlm.nih.gov/pubmed/3342229).
- Huan, Y., Kong, Q., Mou, H., & Yi, H. (2020). Antimicrobial peptides: Classification, design, application and research Progress in multiple fields. Frontiers in Microbiology, 11, 582779. https://doi.org/10.3389/fmicb.2020.582779.
- Huang, J., Buboltz, J. T., & Feigenson, G. W. (1999). Maximum solubility of cholesterol in phosphatidylcholine and phosphatidylethanolamine bilayers. *Biochimica et Biophysica Acta*, 1417(1), 89–100. https://doi.org/10.1016/s0005-2736(98)00260-0.
- Ikonen, E., & Jansen, M. (2008). Cellular sterol trafficking and metabolism: Spotlight on structure. Current Opinion in Cell Biology, 20(4), 371–377. https://doi.org/10.1016/j. ceb.2008.03.017.
- Jing, H., Wang, Y., Desai, P. R., Ramamurthi, K. S., & Das, S. (2020). Lipid flip-flop and desorption from supported lipid bilayers is independent of curvature. *PLoS One*, 15(12), e0244460. https://doi.org/10.1371/journal.pone.0244460.
- Johansen, N. T., Pedersen, M. C., Porcar, L., Martel, A., & Arleth, L. (2018). Introducing SEC-SANS for studies of complex self-organized biological systems. Acta Crystallographica Section D: Structural Biology, 74(Pt 12), 1178–1191. https://doi.org/10. 1107/S2059798318007180.
- John, K., Kubelt, J., Muller, P., Wustner, D., & Herrmann, A. (2002). Rapid transbilayer movement of the fluorescent sterol dehydroergosterol in lipid membranes. *Biophysical Journal*, 83(3), 1525–1534. https://doi.org/10.1016/S0006-3495(02)73922-2.
- Jones, J. D., & Thompson, T. E. (1989). Spontaneous phosphatidylcholine transfer by collision between vesicles at high lipid concentration. *Biochemistry*, 28(1), 129–134. https://doi.org/10.1021/bi00427a019.
- Kaplan, M. R., & Simoni, R. D. (1985). Intracellular transport of phosphatidylcholine to the plasma membrane. *The Journal of Cell Biology*, 101(2), 441–445 (Retrieved from http:// www.ncbi.nlm.nih.gov/pubmed/4040519).
- Khakbaz, P., & Klauda, J. B. (2015). Probing the importance of lipid diversity in cell membranes via molecular simulation. *Chemistry and Physics of Lipids*, 192, 12–22. https://doi.org/10.1016/j.chemphyslip.2015.08.003.
- Kobayashi, T., & Menon, A. K. (2018). Transbilayer lipid asymmetry. *Current Biology*, 28(8), R386–R391. https://doi.org/10.1016/j.cub.2018.01.007.
- Kucerka, N., Nieh, M. P., & Katsaras, J. (2011). Fluid phase lipid areas and bilayer thicknesses of commonly used phosphatidylcholines as a function of temperature. *Biochimica et Biophysica Acta*, 1808(11), 2761–2771. https://doi.org/10.1016/j.bbamem.2011.07.022.
- Laidler, K. J., & King, M. C. (1983). The development of transition-state theory. Journal of Physical Chemistry, 87, 2657–2664.
- Lev, S. (2006). Lipid homoeostasis and Golgi secretory function. *Biochemical Society Transactions*, 34(Pt 3), 363–366. https://doi.org/10.1042/BST0340363.
- Lev, S. (2010). Non-vesicular lipid transport by lipid-transfer proteins and beyond. *Nature Reviews. Molecular Cell Biology*, 11(10), 739–750. https://doi.org/10.1038/nrm2971.
- Leventis, R., & Silvius, J. R. (2001). Use of cyclodextrins to monitor transbilayer movement and differential lipid affinities of cholesterol. *Biophysical Journal*, 81(4), 2257–2267. https://doi.org/10.1016/S0006-3495(01)75873-0.
- Lewis-Laurent, A., Doktorova, M., Heberle, F. A., & Marquardt, D. (2021). Vesicle viewer: Online analysis of small angle scattering from lipid vesicles. *Biophysical Journal*, (ChemRxiv. Cambridge: Cambridge Open Engage; 2021; This content is a preprint and has not been peer-reviewed).

- Liu, J., & Conboy, J. C. (2005). 1,2-diacyl-phosphatidylcholine flip-flop measured directly by sum-frequency vibrational spectroscopy. *Biophysical Journal*, 89(4), 2522–2532. https://doi.org/10.1529/biophysj.105.065672.
- Liu, Y., Kelley, E. G., Batchu, K. C., Porcar, L., & Perez-Salas, U. (2020). Creating asymmetric phospholipid vesicles via exchange with lipid-coated silica nanoparticles. *Langmuir*, 36(30), 8865–8873. https://doi.org/10.1021/acs.langmuir.0c01188.
- Liu, S. L., Sheng, R., Jung, J. H., Wang, L., Stec, E., O'Connor, M. J., et al. (2017). Orthogonal lipid sensors identify transbilayer asymmetry of plasma membrane cholesterol. *Nature Chemical Biology*, 13(3), 268–274. https://doi.org/10.1038/nchembio.2268.
- Lohner, K. (2017). Membrane-active antimicrobial peptides as template structures for novel antibiotic agents. *Current Topics in Medicinal Chemistry*, 17(5), 508–519.
- London, E. (2019). Membrane structure-function insights from asymmetric lipid vesicles. *Accounts of Chemical Research*, 52(8), 2382–2391. https://doi.org/10.1021/acs.accounts. 9b00300.
- Luchini, A., Delhom, R., Deme, B., Laux, V., Moulin, M., Haertlein, M., et al. (2018). The impact of deuteration on natural and synthetic lipids: A neutron diffraction study. *Colloids and Surfaces. B, Biointerfaces*, 168, 126–133. https://doi.org/10.1016/j.colsurfb. 2018.02.009.
- Lund, R., Willner, L., Stellbrink, J., Lindner, P., & Richter, D. (2006). Logarithmic chain-exchange kinetics of diblock copolymer micelles. *Physical Review Letters*, 96(6) (068302. Retrieved from http://www.ncbi.nlm.nih.gov/pubmed/16606054).
- Lusis, A. J. (2000). Atherosclerosis. Nature, 407(6801), 233–241. https://doi.org/10. 1038/35025203.
- Ly, H. V., & Longo, M. L. (2004). The influence of short-chain alcohols on interfacial tension, mechanical properties, area/molecule, and permeability of fluid lipid bilayers. *Biophysical Journal*, 87(2), 1013–1033. https://doi.org/10.1529/biophysj.103.034280.
- Mahieu, E., & Gabel, F. (2018). Biological small-angle neutron scattering: Recent results and development. Acta Crystallographica Section D: Structural Biology, 74(Pt 8), 715–726. https://doi.org/10.1107/S2059798318005016.
- Maric, S., Lind, T. K., Raida, M. R., Bengtsson, E., Fredrikson, G. N., Rogers, S., et al. (2019). Time-resolved small-angle neutron scattering as a probe for the dynamics of lipid exchange between human lipoproteins and naturally derived membranes. *Scientific Reports*, 9(1), 7591. https://doi.org/10.1038/s41598-019-43713-6.
- Markones, M., Drechsler, C., Kaiser, M., Kalie, L., Heerklotz, H., & Fiedler, S. (2018). Engineering asymmetric lipid vesicles: Accurate and convenient control of the outer leaflet lipid composition. *Langmuir*, 34(5), 1999–2005. https://doi.org/10.1021/acs.langmuir.7b03189.
- Markones, M., Fippel, A., Kaiser, M., Drechsler, C., Hunte, C., & Heerklotz, H. (2020). Stairway to asymmetry: Five steps to lipid-asymmetric Proteoliposomes. *Biophysical Journal*, 118(2), 294–302. https://doi.org/10.1016/j.bpj.2019.10.043.
- Marquardt, D., Heberle, F. A., Miti, T., Eicher, B., London, E., Katsaras, J., et al. (2017). 1H NMR shows slow phospholipid Flip-flop in gel and fluid bilayers. *Langmuir*. https://doi.org/10.1021/acs.langmuir.6b04485.
- Marrink, S. J., Corradi, V., Souza, P. C. T., Ingolfsson, H. I., Tieleman, D. P., & Sansom, M. S. P. (2019). Computational modeling of realistic cell membranes. Chemical Reviews, 119(9), 6184–6226. https://doi.org/10.1021/acs.chemrev.8b00460.
- Marx, L., Frewein, M. P. K., Semeraro, E. F., Rechberger, G. N., Lohner, K., Porcar, L., et al. (2021). Antimicrobial peptide activity in asymmetric bacterial membrane mimics. *Faraday Discussions*. https://doi.org/10.1039/D1FD00039J.
- Marx, L., Semeraro, E. F., Mandl, J., Kremser, J., Frewein, M. P., Malanovic, N., et al. (2021). Bridging the antimicrobial activity of two Lactoferricin derivatives in E. coli and lipid-only membranes. *Frontiers in Medical Technology*, 3(2). https://doi.org/10.3389/finedt.2021.625975.

Matencio, A., Navarro-Orcajada, S., Gonzalez-Ramon, A., Garcia-Carmona, F., & Lopez-Nicolas, J. M. (2020). Recent advances in the treatment of Niemann pick disease type C: A mini-review. *International Journal of Pharmaceutics*, 584, 119440. https://doi.org/10.1016/j.ijpharm.2020.119440.

- Maxfield, F. R., & Tabas, I. (2005). Role of cholesterol and lipid organization in disease. *Nature*, 438(7068), 612–621. https://doi.org/10.1038/nature04399.
- McLean, L. R., & Phillips, M. C. (1981). Mechanism of cholesterol and phosphatidylcholine exchange or transfer between unilamellar vesicles. *Biochemistry*, 20(10), 2893–2900. https://doi.org/10.1021/bi00513a028.
- Mellman, I., & Emr, S. D. (2013). A Nobel prize for membrane traffic: Vesicles find their journey's end. The Journal of Cell Biology, 203(4), 559–561. https://doi.org/10.1083/ jcb.201310134.
- Menon, A. K. (2018). Sterol gradients in cells. Current Opinion in Cell Biology, 53, 37–43. https://doi.org/10.1016/j.ceb.2018.04.012.
- Mondal, M., Mesmin, B., Mukherjee, S., & Maxfield, F. R. (2009). Sterols are mainly in the cytoplasmic leaflet of the plasma membrane and the endocytic recycling compartment in CHO cells. *Molecular Biology of the Cell*, 20(2), 581–588. https://doi.org/10.1091/mbc.E08-07-0785.
- Moulin, M., Strohmeier, G. A., Hirz, M., Thompson, K. C., Rennie, A. R., Campbell, R. A., et al. (2018). Perdeuteration of cholesterol for neutron scattering applications using recombinant Pichia pastoris. *Chemistry and Physics of Lipids*, 212, 80–87. https://doi.org/10.1016/j.chemphyslip.2018.01.006.
- Nakano, M. (2019). Evaluation of Interbilayer and Transbilayer transfer dynamics of phospholipids using time-resolved small-angle neutron scattering. *Chemical & Pharmaceutical Bulletin (Tokyo)*, 67(4), 316–320. https://doi.org/10.1248/cpb.c18-00942.
- Nakano, M., Fukuda, M., Kudo, T., Endo, H., & Handa, T. (2007). Determination of interbilayer and transbilayer lipid transfers by time-resolved small-angle neutron scattering. *Physical Review Letters*, *98*(23). https://doi.org/10.1103/Physrevlett.98.238101.
- Nakano, M., Fukuda, M., Kudo, T., Matsuzaki, N., Azuma, T., Sekine, K., et al. (2009). Flip-flop of phospholipids in vesicles: Kinetic analysis with time-resolved small-angle neutron scattering. *The Journal of Physical Chemistry*. B, 113(19), 6745–6748. https://doi.org/10.1021/jp900913w.
- Nakano, M., Fukuda, M., Kudo, T., Miyazaki, M., Wada, Y., Matsuzaki, N., et al. (2009). Static and dynamic properties of phospholipid bilayer nanodiscs. *Journal of the American Chemical Society*, 131(23), 8308–8312. https://doi.org/10.1021/ja9017013.
- Nakao, H., Kimura, Y., Sakai, A., Ikeda, K., & Nakano, M. (2021). Development of membrane-insertable lipid scrambling peptides: A time-resolved small-angle neutron scattering study. Structural Dynamics, 8(2), 024301. https://doi.org/10.1063/4.0000045.
- Nguyen, M. H. L., DiPasquale, M., Rickeard, B. W., Doktorova, M., Heberle, F. A., Scott, H. L., et al. (2019). Peptide-induced lipid Flip-flop in asymmetric liposomes measured by small angle neutron scattering. *Langmuir*, *35*(36), 11735–11744. https://doi.org/10.1021/acs.langmuir.9b01625.
- Nguyen, M. H. L., DiPasquale, M., Rickeard, B. W., Stanley, C. B., Kelley, E. G., & Marquardt, D. (2019). Methanol accelerates DMPC Flip-flop and transfer: A SANS study on lipid dynamics. *Biophysical Journal*, 116(5), 755–759. https://doi.org/10.1016/j.bpj.2019.01.021.
- Nguyen, M. H. L., DiPasquale, M., Rickeard, B. W., Yip, C. G., Greco, K. N., Kelley, E. G., et al. (2021). Time-resolved SANS reveals pore-forming peptides cause rapid lipid reorganization. *New Journal of Chemistry*, 45(1), 447–456. https://doi.org/ 10.1039/D0NJ04717A.
- Nickels, J. D., Chatterjee, S., Stanley, C. B., Qian, S., Cheng, X., Myles, D. A. A., et al. (2017). The in vivo structure of biological membranes and evidence for lipid domains. *PLoS Biology*, *15*(5), e2002214. https://doi.org/10.1371/journal.pbio.2002214.

- Nickels, J. D., Cheng, X., Mostofian, B., Stanley, C., Lindner, B., Heberle, F. A., et al. (2015). Mechanical properties of Nanoscopic lipid domains. *Journal of the American Chemical Society*, 137(50), 15772–15780. https://doi.org/10.1021/jacs.5b08894.
- Nicolson, G. L. (2014). The fluid-mosaic model of membrane structure: Still relevant to understanding the structure, function and dynamics of biological membranes after more than 40 years. *Biochimica et Biophysica Acta*, 1838(6), 1451–1466. https://doi.org/10.1016/j.bbamem.2013.10.019.
- Nielsen, J. E., Bjørnestad, V. A., Pipich, V., Jenssen, H., & Lund, R. (2021). Beyond structural models for the mode of action: How natural antimicrobial peptides affect lipid transport. *Journal of Colloid and Interface Science*, 582, 793–802. https://doi.org/10.1016/j.jcis. 2020.08.094.
- Nielsen, J. E., Prévost, S. F., Jenssen, H., & Lund, R. (2020). Impact of antimicrobial peptides on E. coli-mimicking lipid model membranes: Correlating structural and dynamic effects using scattering methods. Faraday Discussions. https://doi.org/10.1039/D0FD00046A.
- Nyholm, T. K. M., Jaikishan, S., Engberg, O., Hautala, V., & Slotte, J. P. (2019). The affinity of sterols for different phospholipid classes and its impact on lateral segregation. *Biophysical Journal*, 116(2), 296–307. https://doi.org/10.1016/j.bpj.2018.11.3135.
- Opdenkamp, J. A. F. (1979). Lipid asymmetry in membranes. *Annual Review of Biochemistry*, 48, 47–71. https://doi.org/10.1146/Annurev.Bi.48.070179.000403.
- Parisio, G., Sperotto, M. M., & Ferrarini, A. (2012). Flip-flop of steroids in phospholipid bilayers: Effects of the chemical structure on transbilayer diffusion. *Journal of the American Chemical Society*, 134(29), 12198–12208. https://doi.org/10.1021/ja304007t.
- Porcar, L., & Gerelli, Y. (2020). On the lipid flip-flop and phase transition coupling. *Soft Matter*, 16(33), 7696–7703. https://doi.org/10.1039/d0sm01161d.
- Poznansky, M. J., & Lange, Y. (1978). Transbilayer movement of cholesterol in phospholipid vesicles under equilibrium and non-equilibrium conditions. *Biochimica et Biophysica Acta*, 506(2), 256–264 (Retrieved from http://www.ncbi.nlm.nih.gov/pubmed/620032).
- Qian, S., Sharma, V. K., & Clifton, L. A. (2020). Understanding the structure and dynamics of complex biomembrane interactions by neutron scattering techniques. *Langmuir*, 36(50), 15189–15211. https://doi.org/10.1021/acs.langmuir.0c02516.
- Qiu, N., Li, X., & Liu, J. (2017). Application of cyclodextrins in cancer treatment. Journal of Inclusion Phenomena and Macrocyclic Chemistry, 89(3), 229–246. https://doi.org/10.1007/ s10847-017-0752-2.
- Rickeard, B. W., Nguyen, M. H. L., DiPasquale, M., Yip, C. G., Baker, H., Heberle, F. A., et al. (2020). Transverse lipid organization dictates bending fluctuations in model plasma membranes. *Nanoscale*, 12(3), 1438–1447. https://doi.org/10.1039/c9nr07977g.
- Rodrigueza, W. V., Wheeler, J. J., Klimuk, S. K., Kitson, C. N., & Hope, M. J. (1995). Transbilayer movement and net flux of cholesterol and cholesterol sulfate between liposomal membranes. *Biochemistry*, 34(18), 6208–6217. https://doi.org/10. 1021/Bi00018a025.
- Ryan, R. O. (2010). Nanobiotechnology applications of reconstituted high density lipoprotein. *Journal of Nanobiotechnology*, 8(1), 28. https://doi.org/10.1186/1477-3155-8-28.
- Sahoo, S., Adamiak, M., Mathiyalagan, P., Kenneweg, F., Kafert-Kasting, S., & Thum, T. (2021). Therapeutic and diagnostic translation of extracellular vesicles in cardiovascular diseases: Roadmap to the clinic. *Circulation*, 143(14), 1426–1449. https://doi. org/10.1161/CIRCULATIONAHA.120.049254.
- Sapay, N., Bennett, W. F. D., & Tieleman, D. P. (2009). Thermodynamics of flip-flop and desorption for a systematic series of phosphatidylcholine lipids. *Soft Matter*, 5(17), 3295–3302. https://doi.org/10.1039/b902376c.
- Schroeder, F., Frolov, A. A., Murphy, E. J., Atshaves, B. P., Jefferson, J. R., Pu, L. X., et al. (1996). Recent advances in membrane cholesterol domain dynamics and intracellular cholesterol trafficking. *Proceedings of the Society for Experimental Biology and Medicine*, 213(2), 150–177.

Scott, H. L., Kennison, K. B., Enoki, T. A., Doktorova, M., Kinnun, J. J., Heberle, F. A., et al. (2021). Model membrane systems used to study plasma membrane lipid asymmetry. Symmetry, 13(8), 1356. https://doi.org/10.3390/sym13081356.

- Scott, H. L., Skinkle, A., Kelley, E. G., Waxham, M. N., Levental, I., & Heberle, F. A. (2019). On the mechanism of bilayer separation by extrusion, or why your LUVs are not really Unilamellar. *Biophysical Journal*, 117(8), 1381–1386. https://doi.org/10.1016/j.bpj.2019.09.006.
- Seelig, A., & Seelig, J. (1977). Effect of a single cis double bond on the structures of a phospholipid bilayer. *Biochemistry*, 16(1), 45–50. https://doi.org/10.1021/bi00620a008.
- Semeraro, E. F., Devos, J. M., Porcar, L., Forsyth, V. T., & Narayanan, T. (2017). In vivo analysis of the Escherichia coli ultrastructure by small-angle scattering. *IUCrJ*, 4(Pt 6), 751–757. https://doi.org/10.1107/S2052252517013008.
- Semeraro, E. F., Marx, L., Frewein, M. P. K., & Pabst, G. (2021). Increasing complexity in small-angle X-ray and neutron scattering experiments: From biological membrane mimics to live cells. Soft Matter, 17(2), 222–232. https://doi.org/10.1039/c9sm02352f.
- Semeraro, E. F., Marx, L., Mandl, J., Frewein, M. P. K., Scott, H. L., Prevost, S., et al. (2021). Evolution of the analytical scattering model of live Escherichia coli. *Journal of Applied Crystallography*, 54(Pt 2), 473–485. https://doi.org/10.1107/S1600576721000169.
- Simons, K., & Ikonen, E. (1997). Functional rafts in cell membranes. *Nature*, 387(6633), 569–572. https://doi.org/10.1038/42408.
- Sivia, D. S. (2011). Elementary scattering theory: For X-ray and neutron users. In Oxford. New York: Oxford University Press.
- Solanko, L. M., Sullivan, D. P., Sere, Y. Y., Szomek, M., Lunding, A., Solanko, K. A., et al. (2018). Ergosterol is mainly located in the cytoplasmic leaflet of the yeast plasma membrane. *Traffic*, 19(3), 198–214. https://doi.org/10.1111/tra.12545.
- Sprong, H., van der Sluijs, P., & van Meer, G. (2001). How proteins move lipids and lipids move proteins. *Nature Reviews. Molecular Cell Biology*, 2(7), 504–513. https://doi.org/10. 1038/35080071.
- StClair, J. R., Wang, Q., Li, G., & London, E. (2017). Preparation and physical properties of asymmetric model membrane vesicles. In R. Epand, & J. M. Ruysschaert (Eds.), Springer series in biophysics: Vol. 19. The biophysics of cell membranes Springer.
- Steck, T. L., & Lange, Y. (2018). Transverse distribution of plasma membrane bilayer cholesterol: Picking sides. *Traffic*, 19(10), 750–760. https://doi.org/10.1111/tra.12586.
- Steck, T. L., Ye, J., & Lange, Y. (2002). Probing red cell membrane cholesterol movement with cyclodextrin. *Biophysical Journal*, 83(4), 2118–2125. https://doi.org/10.1016/ S0006-3495(02)73972-6.
- Stevens, M. M., Honerkamp-Smith, A. R., & Keller, S. L. (2010). Solubility limits of cholesterol, Lanosterol, Ergosterol, Stigmasterol, and beta-Sitosterol in electroformed lipid vesicles. Soft Matter, 6(23), 5882–5890. https://doi.org/10.1039/c0sm00373e.
- Stone, M. B., Shelby, S. A., Nunez, M. F., Wisser, K., & Veatch, S. L. (2017). Protein sorting by lipid phase-like domains supports emergent signaling function in B lymphocyte plasma membranes. *eLife*, 6. https://doi.org/10.7554/eLife.19891.
- Strott, C. A., & Higashi, Y. (2003). Cholesterol sulfate in human physiology: what's it all about? Journal of Lipid Research, 44(7), 1268–1278. https://doi.org/10.1194/jlr. R300005-JLR200.
- Sud, M., Fahy, E., Cotter, D., Brown, A., Dennis, E. A., Glass, C. K., et al. (2007). LMSD: LIPID MAPS structure database. *Nucleic Acids Research*, 35(Database issue), D527–D532. https://doi.org/10.1093/nar/gkl838.
- Sugiyama, M., Yagi, H., Yamaguchi, T., Kumoi, K., Hirai, M., Oba, Y., et al. (2014). Conformational characterization of a protein complex involving intrinsically disordered protein by small-angle neutron scattering using the inverse contrast matching method:

- A case study of interaction between [alpha]-synuclein and PbaB tetramer as a model chaperone. *Journal of Applied Crystallography*, 47(1), 430–435. https://doi.org/10.1107/S1600576713033475.
- Svergun, D. I. (2010). Small-angle X-ray and neutron scattering as a tool for structural systems biology. *Biological Chemistry*, 391(7), 737–743. https://doi.org/10.1515/BC. 2010.093.
- Svergun, D. I., Feigin, L. A., & Taylor, G. W. (1987). Structure analysis by small-angle X-ray and neutron scattering. New York: Plenum Press.
- Thomson, J. F. (1960). Physiological effects of D20 in mammals. Annals of the New York Academy of Sciences, 84, 736–744. https://doi.org/10.1111/j.1749-6632.1960.tb39105.x.
- Treece, B. W., Kienzle, P. A., Hoogerheide, D. P., Majkrzak, C. F., Losche, M., & Heinrich, F. (2019). Optimization of reflectometry experiments using information theory. *Journal of Applied Crystallography*, 52(Pt 1), 47–59. https://doi.org/10.1107/S1600576718017016.
- van Meer, G. (1989). Lipid traffic in animal cells. *Annual Review of Cell Biology*, 5, 247–275. https://doi.org/10.1146/annurev.cb.05.110189.001335.
- van Meer, G., Voelker, D. R., & Feigenson, G. W. (2008). Membrane lipids: Where they are and how they behave. *Nature Reviews. Molecular Cell Biology*, 9(2), 112–124. https://doi.org/10.1038/nrm2330.
- Vance, J. E., Aasman, E. J., & Szarka, R. (1991). Brefeldin a does not inhibit the movement of phosphatidylethanolamine from its sites for synthesis to the cell surface. *The Journal of Biological Chemistry*, 266(13), 8241–8247 (Retrieved from http://www.ncbi.nlm.nih. gov/pubmed/2022641).
- Vishnepolsky, B., Zaalishvili, G., Karapetian, M., Nasrashvili, T., Kuljanishvili, N., Gabrielian, A., et al. (2019). De novo design and in vitro testing of antimicrobial peptides against gram-negative bacteria. *Pharmaceuticals (Basel)*, 12(2). https://doi.org/10.3390/ph12020082.
- Voelker, D. R. (1990). Lipid transport pathways in mammalian cells. *Experientia*, 46(6), 569–579 (Retrieved from http://www.ncbi.nlm.nih.gov/pubmed/2193820).
- Voelker, D. R. (1991). Organelle biogenesis and intracellular lipid transport in eukaryotes. *Microbiological Reviews*, 55(4), 543–560. https://doi.org/10.1128/mr.55.4.543-560.1991.
- Wah, B., Breidigan, J. M., Adams, J., Horbal, P., Garg, S., Porcar, L., et al. (2017). Reconciling differences between lipid transfer in free-standing and solid supported membranes: A time resolved small angle neutron scattering study. *Langmuir*, 33, 3384–3394. https://doi.org/10.1021/acs.langmuir.6b04013.
- Waldie, S., Moulin, M., Porcar, L., Pichler, H., Strohmeier, G. A., Skoda, M., et al. (2019). The production of Matchout-deuterated cholesterol and the study of bilayer-cholesterol interactions. *Scientific Reports*, 9(1), 5118. https://doi.org/10.1038/s41598-019-41439-z.
- Weiner, M. D., & Feigenson, G. W. (2019). Molecular dynamics simulations reveal leaflet coupling in compositionally asymmetric phase-separated lipid membranes. *The Journal of Physical Chemistry*. B, 123(18), 3968–3975. https://doi.org/10.1021/acs.jpcb.9b03488.
- Wimley, W. C., & Hristova, K. (2011). Antimicrobial peptides: Successes, challenges and unanswered questions. *The Journal of Membrane Biology*, 239(1–2), 27–34. https://doi.org/10.1007/s00232-011-9343-0.
- Wimley, W. C., & Thompson, T. E. (1991). Transbilayer and interbilayer phospholipid exchange in dimyristoylphosphatidylcholine/dimyristoylphosphatidylchanolamine large unilamellar vesicles. *Biochemistry*, 30(6), 1702–1709. https://doi.org/10.1021/bi00220a036.
- Wood, W. G., Igbavboa, U., Muller, W. E., & Eckert, G. P. (2011). Cholesterol asymmetry in synaptic plasma membranes. *Journal of Neurochemistry*, 116(5), 684–689. https://doi. org/10.1111/j.1471-4159.2010.07017.x.

Xia, Y., Li, M., Charubin, K., Liu, Y., Heberle, F. A., Katsaras, J., et al. (2015). Effects of nanoparticle morphology and acyl chain length on spontaneous lipid transfer rates. *Langmuir*, *31*(47), 12920–12928. https://doi.org/10.1021/acs.langmuir.5b03291.

- Xiao, Q., McAtee, C. K., & Su, X. (2021). Phase separation in immune signalling. *Nature Reviews. Immunology*. https://doi.org/10.1038/s41577-021-00572-5.
- Yancey, P. G., Rodrigueza, W. V., Kilsdonk, E. P., Stoudt, G. W., Johnson, W. J., Phillips, M. C., et al. (1996). Cellular cholesterol efflux mediated by cyclodextrins. Demonstration of kinetic pools and mechanism of efflux. *The Journal of Biological Chemistry*, 271(27), 16026–16034. https://doi.org/10.1074/jbc.271.27.16026.
- Yeagle, P. L. (1993). The membrane of cells. New York: Academic Press, Inc.
- Zaccai, N. R., Sandlin, C. W., Hoopes, J. T., Curtis, J. E., Fleming, P. J., Fleming, K. G., et al. (2016). Deuterium labeling together with contrast variation small-angle neutron scattering suggests how Skp captures and releases unfolded outer membrane proteins. Methods in Enzymology, 566, 159–210. https://doi.org/10.1016/bs.mie.2015.06.041.
- Zidovetzki, R., & Levitan, I. (2007). Use of cyclodextrins to manipulate plasma membrane cholesterol content: Evidence, misconceptions and control strategies. *Biochimica et Biophysica Acta*, 1768(6), 1311–1324. https://doi.org/10.1016/j.bbamem.2007.03.026.